THESIS FOR THE DEGREE OF DOCTOR OF PHILOSOPHY

Multiscale Simulation Methods for Thermoelectric Generators

OLLE HÖGBLOM

Department of Chemistry and Chemical Engineering
CHALMERS UNIVERSITY OF TECHNOLOGY
Gothenburg, Sweden 2016

Multiscale Simulation Methods for Thermoelectric Generators
OLLE HÖGBLOM

ISBN: 978-91-7597-363-0

Doktorsavhandlingar vid Chalmers tekniska högskola
Ny serie nr 4044
ISSN 0346-718X

Division of Chemical engineering
Department of Chemistry and Chemical Engineering
Chalmers University of Technology
SE-412 96 Gothenburg
Sweden
Telephone: +46(0)31-7721000

Chalmers Reproservice
Gothenburg, Sweden 2016

Multiscale Simulation Methods for Thermoelectric Generators

OLLE HÖGBLOM
Department of Chemistry and Chemical Engineering
Chalmers University of Technology

ABSTRACT

Rising energy prices and greater environmental awareness, along with stringent emissions legislation, in the automotive industry make it possible to introduce techniques in the aftertreatment system that have previously been unprofitable. One such technique, studied here, is heat recovery from exhaust gases using thermoelectric generators.

The design of thermoelectric modules and heat exchangers for thermoelectric generation relies, to a large extent, on simulation tools. Thermoelectric phenomena are well known, and several researchers have used first principle simulation to solve for thermoelectric generation in thermoelectric pairs and single modules. In order to obtain predictions that agree with measurements, knowledge of not only temperature-dependent material but also internal thermal and electrical contact resistances is required. A method that enables accurate quantification of contact resistances inside thermoelectric generators and which gives detailed insight into how these reduce module performance has been developed within the scope of this research. When implementing these resistances in first principle simulations, excellent agreement between measured and simulated performance has been achieved.

First principle simulations allow great insight into thermoelectric performance and provide details, such as local current distribution, that are hard to measure or obtain with other methods and are great, for example, when designing modules. First principle models, on the other hand, are computationally too demanding when used to design heat exchangers that contain a large system of modules. Therefore, a novel framework for characterization and simulation of thermoelectric generator systems that allows for accurate and efficient prediction of electric and thermal performance has been developed in this research. When used in conjunction with CFD analysis, this framework allows for efficient modelling of electrical and thermal performance without relaxing the important two-way coupling of energy transport. This efficiency comes from the fact that the modelling does not require full resolution as first principle simulations do. Therefore it solves the scale separation problem and allows for multiphysics simulation with just a minor increase in computational power.

All simulations were validated with experiments on different levels, both for individual modules, small systems of modules, and, finally, engine bench tests were used to validate a full-scale heat exchanger prototype containing a large number of modules and a complex fluid flow.

Keywords: Thermoelectrics, Contact resistances, CFD, Exhaust gas heat recovery, subgrid modelling

LIST OF PUBLICATIONS

This thesis is based on the following enclosed papers:

Paper I **CFD Modeling of Thermoelectric Generators in Automotive EGR Cooler**

Olle Högblom and Ronnie Andersson

American Institute of Physics Conference Series 2011. 1449: p. 497-500

Paper II **Analysis of Thermoelectric Generator Performance by Use of Simulations and Experiments**

Olle Högblom and Ronnie Andersson

Journal of Electronic Materials, 2014. **43**(6): p. 2247-2254.

Paper III **A Simulation Framework for Prediction of Thermoelectric Generator System Performance**

Olle Högblom and Ronnie Andersson

Submitted for publication in Applied Energy 2016

Paper IV **Simulations and Measurements of an Automotive TEG-EGR Cooler**

Olle Högblom and Ronnie Andersson

In manuscript

Relevant publications not included in this thesis:

V **E4-Mistra, a Research Program for the Development of an Energy Efficient Low Emission Exhaust Aftertreatment System for Heavy Duty Vehicles**

Edvardsson J., Westberg H., Dawody J., Andersson L., Härelind Ingelsten H., Kannisto H., Gunnarsson F., Palmqvist A., Heijl R., Ma Y., Cederkrantz D., Andersson R., Högblom O., Pettersson L. J., Karatzas X., Granlund M. Z., Larsson P. O., Holmgren L. and Andreasson F.

World Renewable Energy Forum, WREF 2012, Conference proceedings, p. 4530-4536, ISBN/ISSN: 978-162276092-3

VI **An integrated system for energy efficient exhaust after-treatment for heavy-duty vehicles**

Dawody, J., Andersson, L., Pettersson, L., Granlund, M., Härelind, H., Gunnarsson, F., Palmqvist, A., Heijl, R., Andersson, R., Högblom, O., Holmgren, L., Larsson, P. and Andreasson, F.

World Renewable Energy Congress, WREC 2014, Renewable Energy in the Service of Mankind Vol I, p. 133-143, ISBN/ISSN: 978-3-319-17776-2

CONTRIBUTION REPORT

Paper I I coded the UDF, performed simulations and, together with the co-author, interpreted the results and wrote the paper.

Paper II I designed and built the experimental setup and performed measurements. I performed the simulations and, together with the co-author, interpreted the results and wrote the paper.

Paper III I designed and built the experimental setup, performed measurements, and analyzed the results. I performed the simulations and developed the models and, together with the co-author, interpreted the results and wrote the paper.

Paper IV I performed simulations and, together with the co-author, interpreted the results and wrote the paper.

ACKNOWLEDGEMENTS

I would like to thank Assoc. prof. Ronnie Andersson and Prof. Bengt Andersson for giving me the opportunity to do my PhD studies at Chemical Engineering, and for all their guidance and support during the project.

I would also like to thank all the members of E4-Mistra for productive and inspiring program meetings and a special thanks to Lennart Holmgren for providing equipment, practical help, and many valuable discussions during the work.

All my colleagues and friends at Chemical Engineering are also gratefully acknowledged and a special thanks to my colleague, office mate, and good friend Soheil Soltani for extensive help during the project and many valuable discussions.

Finally I would like to thank my family and friends for being supportive and letting me spend many late nights in my office.

This work was financially supported by the Swedish Foundation for Strategic Environmental Research through the E4-Mistra program and they are gratefully acknowledged.

The simulations were conducted on the computer cluster at Chalmers University of Technology, supported by the Swedish National Infrastructure for Computing, SNIC.

TABLE OF CONTENTS

Nomenclature

A	cross sectional area, m^2
c_p	specific heat capacity, J kg^{-1} K^{-1}
h	thermal contact conductance, m^2 K W^{-1}
I	current, A
J	current density, A m^{-2}
P	electric power, W
Q	heat per unit volume, W m^{-3}
q	heat flux, W m^{-2}
R	electric resistance, Ω
r	thermal contact resistance, m^2 K W^{-1}
SS	normalized sum of square errors, -
T	temperature, K
U	potential, V
ZT	figure of merit, -

Greek symbols

α	Seebeck coefficient V K^{-1}
β	regression coefficient
λ	thermal conductivity, W m^{-1} K^{-1}
Π	Peltier coefficient, V
ρ	density, kg m^{-3}
ϱ	electrical contact resistance, Ω m^2
σ	electric conductivity, Ω^{-1} m^{-1}
ς	electric contact conductance, Ω^{-1} m^{-2}
τ	Thomson coefficient, V K^{-1}
Ψ	combined Peltier and Thomson coefficients, V

Subscripts

A	material A
avg	average
B	material B
c	cold side
Fi	Fourier conduction where i = 1, 2
h	hot side
i, j	index
int	internal
L	load
n	n-doped material
p	p- doped material
PTi	Peltier & Thomson where i = 1, 2
Ri	internal resistance where i = 1, 2, 3
Si	Seebeck where i = 1, 2

1 INTRODUCTION

During the last decade, it has become increasingly clear that climate change together with a shortage of fossil fuel are two of the main threats to the environment and our society today. The transport sector represents about one third of the overall energy consumption in the world, and the source of energy in the sector is completely dominated by fossil fuels [1].

Vehicle manufacturers are constantly striving to lower fuel consumption, and a growing awareness of both fuel costs and the environmental concerns among customers has enhanced this focus even more.

In addition to the demands of manufacturers and customers on fuel consumption, legislation on emission adopted by the EU and the EPA (United States Environmental Protection Agency) is becoming increasingly stringent, and is creating demands for engines and vehicles that consume less fuel [2].

In order to meet carbon dioxide emission limits, it might be possible and perhaps also necessary to introduce new technologies that otherwise might be unprofitable and too expensive to pay for themselves.

Thermoelectric generation (TEG) is one such technique that allows direct conversion of heat into electricity, and it is rising in popularity for heat recuperation applications mainly because of its compactness and robustness without moving parts. Different fields of implementation of TEGs have been reported in the literature, including biomass [3-5], solar energy [6-10], geothermal [11, 12], nuclear [13], and even industrial power plants [14, 15]. Several researchers have also studied thermoelectric recuperation for automotive applications [16-25]. Due to the broad interest in developing technical applications, effort has also been put into developing simulation tools that range from first principle

simulations of small systems [26-30], to full-scale TEG system simulations using simplified models [19, 20], and also coupled system simulations that combine fluid dynamics simulations with thermoelectric models [31].

Thermal and electrical contact resistances inside thermoelectric modules (TEM) influence thermoelectric (TE) performance, and might vary significantly depending on process parameters, and are usually not known [29]. The influence of electrical and thermal contact resistance can have a significant negative impact on module performance, as shown in an investigation by Bjørk et al. [32]. Epling et al. [33] compare contact resistances resulting from the use of different solders, and Tatsuya et al. [34] have studied different interface materials to lower thermal contact resistances.

In the exhaust gas recirculation (EGR) cooler in a diesel engine, a large amount of the heat is, today, already removed from the exhaust gases in order to decrease the combustion temperature and oxygen content in the combustion chamber, and, thereby, the amount of NO_x produced. Some of this energy can be converted to useful electric energy using thermoelectric (TE) elements [18]. Introducing a thermoelectric generator (TEG) in an EGR cooler requires a completely new design of the heat exchanger, which entails several new challenges. The pressure drop in the exhaust gas system should, with a new design, be maintained at a low level, and, at the same time, the heat transfer on the gas side should increase. Several researchers are currently working with thermoelectric generation for heat recuperation in vehicles. Martinez and coworkers have used Computational Fluid Dynamics (CFD) to design heat exchangers and to determine the pressure drop and the heat transfer resistance in TEG systems [35]. Hsu et al. have built prototypes and performed CFD simulations of TEG heat exchangers for exhaust gas aftertreatment [21]. Hsiao et al. have studied two alternative locations for a TEG in vehicles, directly in the exhaust gases and in the radiator [23]. Karri et al. have compared the potential of using quantum well materials, instead of conventional $Bi_2Te_{3,}$ for heat recuperation in the vehicle exhaust stream. They have reported a total fuel savings of up to 3% on a sport utility vehicle, SUV [24].

The implementation of thermoelectric generators in real applications for energy conversion is, currently, limited due to the low efficiency of the

materials, however, with rising fuel prices and stringent emission legislation, the technique has become more and more interesting.

1.1 E4-MISTRA

Mistra is the Swedish Foundation for Strategic Environmental Research, and E4-Mistra is a joint academic and industrial research program in which the goal is energy efficient and low emitting diesel engines for heavy duty diesel engines [36]. The program is based on four different technologies: three technologies aimed at cleaner exhaust gases, and one aimed at lowering fuel consumption. Catalytic reduction of NO_x using hydrocarbons from fuel, highly efficient fuel reformation for more efficient NOx reductions, and innovative particulate filtration over a porous metal filter are all technologies that aim for cleaner exhaust gases. The fourth technology, which this thesis is a part of, aims at increasing the efficiency of a vehicle engine by recovering waste heat from the exhaust gases using thermoelectric power generation.

1.2 OBJECTIVES

The objective of this work is to acquire an understanding of thermoelectric systems and to develop useful simulation models for predicting thermoelectric performance. In order to achieve this goal, a measurement setup for the characterization of modules was designed and built. Two different modelling approaches were used, detailed first principle simulations of TE legs and whole modules and also simplified subgrid models for larger systems of modules. When comparing the first principle simulations with measurements, a method for determining electrical and thermal contact resistances within modules was required and the development of this method also became an objective of this work. The final objective was to develop models that can be used together with CFD for designing and predicting the thermal and thermoelectric performance of EGR heat exchangers, including a large system of integrated modules.

2 THERMOELECTRICS

Thermoelectrics is the science and technology associated with the direct conversion between heat flow and electric current. Thermoelectrics can be used either to create a current from an existing temperature gradient or to create a temperature difference by applying an electric current. Both of these applications have been known since the early 19th century [37]. The technique has the advantage of being robust without any moving parts, and having a long lifetime. The disadvantage of the technique is its low efficiency. Since the discovery of the thermoelectric effect, a lot of research has been conducted in the field, but, nevertheless, the typical efficiency of commercial modules is not more than around 5% [38].

2.1 SEEBECK EFFECT

A semiconductor material can be doped to contain a slightly higher concentration of electrons than a pure semiconductor (*n*-doped), or a slightly lower concentration of electrons than a pure semiconductor (*p*-doped). These extra electrons, or electron "holes," are mobile in the semiconductor, and they are commonly referred to as charge carriers. When a material is exposed to a temperature gradient, these charge carriers are set in motion and start to diffuse from the hot to the cold side. Electric potential is built up, and an electric current can be utilized. This is called the Seebeck effect, and it was discovered by the German physicist Thomas J. Seebeck in 1821 [37].

The potential difference build up is proportional to the temperature difference over the material, and the proportionality constant, α, is called the Seebeck coefficient.

$$\Delta U_{\text{Seebeck}} = \alpha \Delta T \tag{2-1}$$

Since the charge carriers always diffuse from the hot to the cold side, and they are negative for electrons and positive for electron holes, the sign of the Seebeck coefficient is different for the *n*-doped (negative) and *p*-doped (positive) material.

In a differentiated form, Equation (2-1) reads

$$\nabla U_{\text{Seebeck}} = \alpha \nabla T. \tag{2-2}$$

2.2 PELTIER EFFECT

When a current flows in a material, the electrons have a certain level of energy, depending on the material they are transported through. This means that, in the junction between two materials, the electrons have to either take up or release energy, and the junction will subsequently be either cooled or heated. This phenomenon is of the greatest magnitude at the junction between doped semiconductors since there is a large difference in energy for electrons moving in materials with different doping. This effect is known as the Peltier effect. The rate of cooling or heating at the junction between two materials due to the Peltier effect can be written as

$$q_{\text{Peltier}} = (\Pi_{\text{A}} - \Pi_{\text{B}})J \tag{2-3}$$

where J is the current density and Π_{A} and Π_{B} are the Peltier coefficients for the different materials. The difference $\Pi_{\text{A}} - \Pi_{\text{B}}$ is usually written Π_{AB}. Note that the Peltier effect takes place only at the interface and the unit of q_{Peltier} is, therefore, W/m^2.

2.3 THOMSON EFFECT

When the Seebeck coefficient has a temperature dependency and the material is located in a temperature gradient, the electrons moving through the material will have a slight variation in their energy, and,

therefore, heat will be absorbed or released during their movement through the material. This third thermoelectric effect is known as the Thomson effect. It is of less magnitude compared to the Peltier effects, about 1/10 depending on the Seebeck coefficient's temperature dependence in the operating range.

The Thomson effect can be seen as a continuous variant of the Peltier effect that is active inside the TE material, while the Peltier effect only occurs at the interfaces between different materials.

The rate of cooling or heating inside the material due to the Thomson effect is given by

$$Q_{\text{Thomson}} = \tau J \nabla T \tag{2-4}$$

where τ is called the materials Thomson coefficient. Since the Thomson effect is active inside the material, the unit of Q_{Thomson} is W/m^3.

2.4 KELVIN RELATIONSHIPS

The Seebeck, Peltier, and the Thomson effects are closely related. The Peltier effect can be seen as the back-action counterpart of the Seebeck effect; the Seebeck effect builds up a potential difference that pushes a current through a circuit, and the current then causes the Peltier effect to transport heat from the hot to the cold side, thereby, lowering the temperature difference. In a TEG, the Peltier effect is an undesirable side effect.

The close relationship between the Seebeck, Peltier, and Thomson effects can also be seen in their coefficients, which are combined with the Kelvin relations

$$\Pi_{\text{AB}} = \alpha_{\text{AB}} T \tag{2-5}$$

$$\tau = \frac{d\alpha}{dT} T \tag{2-6}$$

When combining Equations (2-4) and (2-6), the resulting equation describes the Thomson effect inside the material, and it also describes the Peltier effect at the interface between two different materials.

$$Q_{Peltier\&Thomson} = TJ\nabla\alpha \tag{2-7}$$

The Peltier effect is nothing but a large and local Thomson effect occurring at the interface where α has a discontinuity.

2.5 JOULE HEATING

When a current flows through a material, some of the electric energy is lost and converted to heat. This is not a pure thermoelectric effect, but it exists in all materials, and it is an important, undesired effect that lowers the performance in both thermoelectric generators and Peltier coolers. This is a non-reversible effect in contrast to the other effects. The potential loss due to Joule heating can be written as

$$\nabla U_{\text{Joule}} = -\frac{J}{\sigma} \tag{2-8}$$

where σ is the electric conductivity of the material and J is the current density.

The amount of electric energy converted to heat as a consequence of ohmic losses can be described by Joule's law

$$q_{\text{Joule}} = UJ \tag{2-9}$$

q_{Joule} is the heat produced per cross sectional area (W/m^2). This equation can further be rewritten in terms of heat per volume, and by using Ohm's law it is given by

$$Q_{\text{Joule}} = \frac{J^2}{\sigma} \tag{2-10}$$

2.6 THERMAL CONDUCTION

A transport of thermal energy occurs in all materials that are exposed to a temperature gradient due to conduction. Conduction in a solid material is based mainly on two phenomena; diffusion and collisions of free electrons, and propagation and collisions of lattice vibrations, so called phonons. Heat conduction in metals is dominated by free electrons, and a large amount of free electrons makes metals good thermal conductors. Electrical insulators, in contrast, have no free electrons, and heat conduction is dominated by phonons. The more structured a material is, and the stronger intermolecular bonds, the better thermal conductor the material is. This is the reason that diamonds are great thermal conductors: the transport of phonons is good in a diamond because of strong intermolecular bonds, and the phonon scattering is low because of the perfectly organized structure.

A semiconductor has movable electrons, and materials with a high Seebeck coefficient usually have a well-organized structure, so lattice vibrations will make a significant contribution to thermal conduction.

The equation that describes pure conduction is usually referred to as Fourier's law and is written

$$q_{\text{Fourier}} = -\lambda \nabla T \tag{2-11}$$

Fourier's law can be rewritten with an accumulation term, and it is then called Fourier's 2nd law or the energy equation for pure conduction. It is then given by

$$\rho c_p \frac{\partial T}{\partial t} = \nabla(\lambda \nabla T) \tag{2-12}$$

2.7 THERMOELECTRIC CONSTITUTIVE EQUATIONS

Combining Equations (2-2) and (2-8) results in an equation that describes the potential field

$$\nabla U = \alpha \nabla T - \frac{J}{\sigma} \tag{2-13}$$

where the potential field is built up from the diffusion of charge carriers in the direction of the temperature gradient (the first term on the right-hand side), and is reduced through ohmic losses (the second term on the right-hand side).

The complete energy equation for the thermoelectric material can be derived from Equations (2-6), (2-10) and (2-12), and it is written

$$\rho c_p \frac{\partial T}{\partial t} = \nabla(\lambda \nabla T) + \frac{J^2}{\sigma} + TJ\nabla\alpha \tag{2-14}$$

The term on the left-hand side is the accumulation term, the first term on the right-hand side is the Fourier conduction, the second term is the Joule heating, and the third term on the right-hand side is the Peltier and Thomson effects.

Equations (2-13) and (2-14) are called the constitutive equations for thermoelectricity, and all the relevant effects are taken into account by solving them with temperature-dependent material data.

Note that the last term in Equation (2-14) is the Peltier and Thomson effects together. In the materials, $\nabla\alpha$ is moderate and a result of a temperature-dependent Seebeck coefficient. This is equivalent to the Thomson effect.

In order to see how this term also describes the Peltier effect, it can be discretized and applied to a small element with thickness Δz located over the interface between two different materials (assuming the gradient is in the z-direction). $q = TJ\frac{\Delta\alpha}{\Delta z}\Delta z$. This equation now describes heat per cross-sectional area within the element and, thereby, the choice of q instead of Q. By letting Δz approach zero, this equation describes the

heat per area over the interface, which is equal to the Peltier effect, i.e. $q = TJ\frac{\Delta\alpha}{\Delta z}\Delta z = \Delta\alpha TJ = \Pi J = q_{\text{Peltier}}$.

2.8 THERMOELECTRIC MATERIALS

A good thermoelectric material has a high Seebeck coefficient, high electric conductivity, and low thermal conductivity. When designing a TE material, there is always a tradeoff between keeping the electric conductivity high and the thermal conductivity low. The reason for this is that electrons are responsible for the transport of both electric current and heat. Heat can also be transported with lattice vibrations, so called phonons, and lowering this contribution to the heat conductivity is of great importance when developing new materials.

Materials like glass have low thermal conductivity due to the unstructured way the material lattice is organized [39]. Phonons are easily scattered, and the thermal conductivity due to lattice vibration is, thereby, minimal. In contrast, glass does not conduct electrons, so it is a poor thermoelectric material. Good thermoelectric materials are crystalline materials that manage to scatter phonons without disrupting electrical conductivity, they should have phonon-scattering properties similar to glass but a crystal structure for conducting electrons. These 'phonon-glass electron-crystal' properties are unusual [40], and there are no reliable theoretical models for designing materials and predicting properties. The best thermoelectric materials known today are crystalline semiconducting materials, and several researchers are working on developing new and improving existing materials by means of, for example, nano inclusions [41, 42] and partial substitution of the base material [43, 44].

Bismuth telluride (Bi_2Te_3) is the most commonly used thermoelectric material, and it was first suggested as a TE material as early as 1954 [45]. Nevertheless, it remains today the best TE material for low temperature conversion. Its thermoelectric properties strongly depend on carrier concentration, crystal size, and crystal orientation, so the material properties are different for Bi_2Te_3 from different manufacturers.

2.9 THERMOELECTRIC DEVICES

A thermoelectric device for power generation or cooling consists of several pairs of *n* and *p* materials. These are connected electrically in series and thermally in parallel. Simplified devices with only one pair for power generation and cooling are shown in Figure 1.

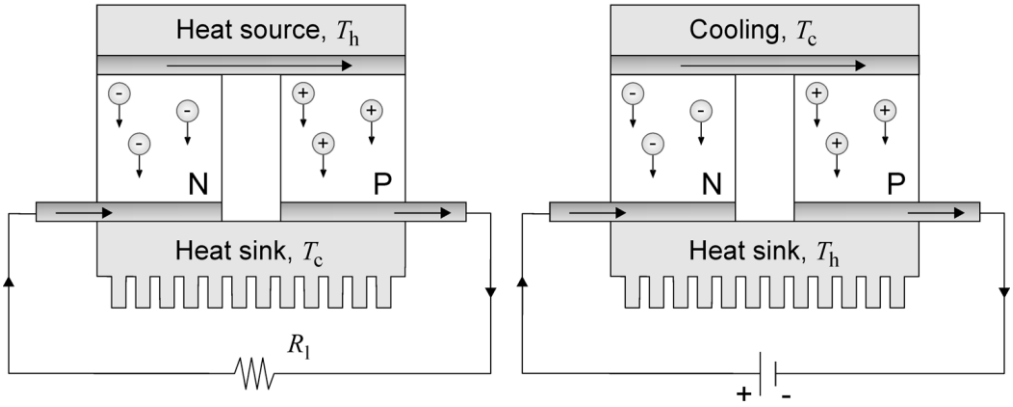

Figure 1. Schematics of a) TE generator and b) TE cooler

For a thermoelectric generator, the efficiency, η, which is the ratio of power delivered by the unit to the heat flow through the module, can be expressed as

$$\eta = \frac{(T_h - T_c)}{T_h} \frac{\left(1 + ZT_{avg}\right)^{1/2} - 1}{\left(1 + ZT_{avg}\right)^{1/2} + T_h/T_c} \tag{2-15}$$

where ZT_{avg} is the figure of merit for the TE pellets which is based on the average temperature within the pellet

$$T_{avg} = (T_h + T_c)/2 \tag{2-16}$$

and the three material key parameters, the Seebeck coefficient α, the electrical conductivity σ, and the thermal conductivity λ.

$$Z = \alpha^2 \sigma / \lambda \tag{2-17}$$

The first part of Equation (2-15), $(T_h - T_c)/T_h$, is the Carnot efficiency. This is the highest theoretically possible efficiency that can be reached. This requires a ZT value close to infinity, which of course is impossible in a real system. There is, however, no theoretical upper limit for the ZT value, but the best thermoelectric materials existing today have a $ZT < 2$. Materials with a $ZT > 2$ have been reported in thin films, but due to problems with the measurement technique, it has been hard to reproduce them in independent studies [39]. A tellurium-based bulk material with a $ZT \approx 2.2$ that looks promising for the automotive industry has recently been discovered [46].

A thermoelectric device typically operates at about 10% of Carnot efficiency. This can be compared to a kitchen refrigerator, which operates at about 30% of Carnot efficiency, and the largest air conditioner for buildings operates at close to 90% of Carnot efficiency [47].

2.10 TE MODULES

In a TE module, the TE pellets are electrically connected in series with small metal plates. These connectors are usually made of copper or aluminum for good electric and thermal conductance. The connectors on the cold side are mounted on a sheet of a ceramic material that is both a good thermal conductor and an electric insulator. A commonly used material is aluminum oxide (Al_2O_3) since it is cheap, stiff, and possesses the right thermal and electrical properties. The thermoelectric pellets are mounted on the metal connectors on the cold side, and they are connected together with additional metal connectors on the hot side. The whole package is then covered with another layer of the ceramic material.

In this research two different TE modules were used. They were both commercial Bi_2Te_3 from Thermonamics Electronics Co., Ltd. One of the modules, TEPH1-12680-0.15, was 80×80 mm, consisted of 126 thermoelectric pairs, and will be referred to as the ‘large module’ in this thesis. The other one, TEP1-1264-1.5, was 40×40mm, consisted of 127 pairs, and will be referred to as the ‘small module’.

The thermoelectric pellets in the large module had a cross-sectional area of 3.60×3.60 mm, and the height of the pellets was 1.35mm. The cross-sectional area of the pellets in the small module was 1.50×1.50 mm and their height was 1.20mm.

On the cold side, the connectors were made of copper and the TE pellets were soldered to the connectors to achieve good contact. On the hot side, the connectors were built directly onto the TE material by spray depositing several thin layers of melted aluminum, so called thermal spraying. Between the connectors on the hot side and the ceramic plate there was a layer of graphite that had to be compressed for the module to work properly.

When using thermoelectric modules for power generation or cooling, it is important to obtain sufficient contact pressure. The modules should be compressed in order to minimize internal contact resistances and to remain mechanically stable. If sufficient contact pressure is not applied, the graphite layer is not working properly and there is a substantial risk for poor thermal contact between the metal connectors on the hot side and the ceramic plate.

2.11 CONTACT RESISTANCES

Between two solid materials, the interface is never in perfect contact. Even if the surfaces look perfectly smooth, there will always be microscopic roughness on the surfaces that will form air-filled voids when the surfaces are pressed together [34, 48]. These voids decrease the surface area that is actually in contact, how much depends on surface roughness, the softness of the materials, and the contact pressure. A soft surface will deform with applied pressure, thereby increasing the effective contact area. If an electric current or a heat flow is conducted through the interface, it will pass through the area that is in good contact. Heat conduction is also possible through the air-filled voids, but the conductivity of air is very low compared to most solid materials, so this will make a minor contribution to the total transferred energy. For a thermal insulator, the contact conductivity might be of the same magnitude as for air, and, in that case, the contact conductivity is negligible. Any electric current will also be concentrated to the microscopic contact areas. The electric conductivity of air can always be negligible, but tunneling phenomena can, however, transfer some current through the air-filled voids [49]. Potential surface coatings, such as oxides or other impurities, might affect both the thermal and the electrical conductivity over an interface. Thermal contact conductance can be

defined in an expression similar to Newton's rate equation for convection as

$$h_{\text{contact}} = \frac{Q_{\text{interface}}/A}{\Delta T_{\text{interface}}} \tag{2-18}$$

where $Q_{\text{interface}}$ is the heat flow over the interface, A is the total interface area, and $\Delta T_{\text{interface}}$ is the temperature difference over the interface. In a similar manner, electrical contact conductance can be defined as

$$\varsigma_{\text{contact}} = \frac{J_{\text{interface}}}{\Delta U_{\text{interface}}} \tag{2-19}$$

where $J_{\text{interface}}$ is the current density over the interface and $\Delta U_{\text{intercafe}}$ is the corresponding potential drop.

Values for contact conductance are usually given in the literature, however, it would be more natural to give them in terms of their inverses, their contact resistances,

$$r_{\text{contact}} = \frac{1}{h_{\text{contact}}} \tag{2-20}$$

and

$$\varrho_{\text{contact}} = \frac{1}{\varsigma_{\text{contact}}}. \tag{2-21}$$

This would be more natural, because they are actually resistances to the transfer of heat and current through the interface.

The magnitude of the thermal contact resistances can be decreased by minimizing the area of the voids, either by smoothing or softening the surfaces, or by increasing contact pressure. Another way to lower contact resistances is to fill the voids with a material with high conductivity. A thin layer of thermal grease or graphite is commonly used to fill the voids

and enhance thermal contacts [34, 50]. Such a material has far better thermal conductivity than air, but much lower than metals.

A common method for lowering electrical contact resistances is to cover the surface with a soft, electrically conducting material that is resistant to oxidization. A technically beneficial but expensive choice of coating material is gold. The thickness of the gold layer is important, and Nagaraju has shown that a gold layer that is too thin will increase rather than decrease contact resistance [49].

Temperature might potentially affect resistances since material properties, such as softness, are temperature-dependent. Thermal expansion might also change contact pressure depending on the system.

When joining materials by soldering, several factors influence the contact resistance at the joint, and perfectly soldered joints should have the potential for very low thermal and electrical contact resistances. When soldering, there is always the risk of trapping air at the interface, which will increase contact resistances, as discussed earlier. It is important to completely wet the surfaces with the molten metal to achieve low contact resistances. Surface roughness, together with the surface tension of the melted metal, are factors that strongly affect the result of soldering [51].

None of the junctions between the different parts inside a TE module (TE pellets, metal connectors, and ceramic plates) have ideal contacts. Since an electrical current must pass through a large number of TE pellets, and, since every pellet has two contact areas, the electrical contact resistance is rarely negligible. The most important contact resistances are the electrical resistances on both sides of thermoelectric pellets, and the thermal resistances between the connectors and the ceramic plates. There may also be thermal contact resistance between the pellets and the metal connectors. The locations of thermal and electrical contact resistances are highlighted in Figure 2.

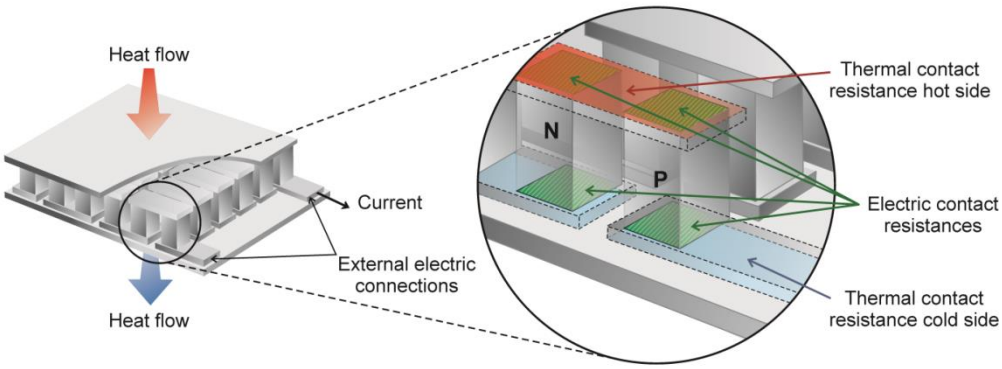

Figure 2. Contact resistances within a TE module

2.12 SYSTEM OF MODULES

There are several different reasons why TEG modules are connected electrically together. Serial connections can, for example, be used to increase the overall voltage delivered by a system. Parallel connections, in contrast, can be used to keep the voltage at a reasonable low, useful level, to increase the current, and to avoid complete power failure if one model is damaged. In real TEG applications, it is therefore common to use a combination of serial and parallel connected modules.

A system of TEG modules that are exposed to different temperature gradients and electrically connected together always produces a lower power output than if the modules were allowed to operate independently. The reason for this becomes clear when studying the PI- and VI-graphs for a TEG module.

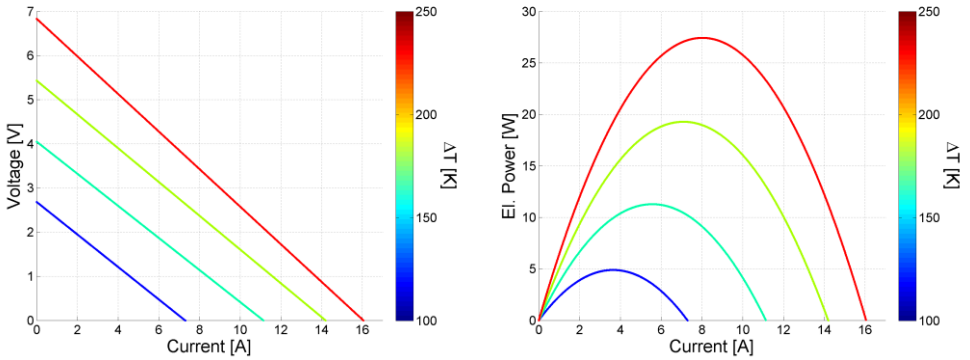

Figure 3. Electric characteristics from a TEG module colored by the temperature difference. a) voltage vs. current and b) power vs. current

The maximum power a module can deliver is naturally dependent on the temperature difference it is exposed to. Figure 3a and b show the VI and PI graphs for the large modules described in Section 2.10 for four different temperature differences. As can be seen, the current resulting in the maximum power output is dependent on the temperature difference.

If modules are connected in series, the current through them must be the same. This can be visualized with an arbitrary vertical line in Figure 3b. It is obvious that two modules at different temperatures cannot simultaneously operate at their maximum power output. If the modules are instead connected in parallel, the voltage over them will be the same, and this can be visualized with a horizontal line in Figure 3a. This results in different currents through the modules, but it can never result in a maximum power output for both modules. If the power output is plotted as a function of the voltage, as shown in Figure 4, this becomes even clearer.

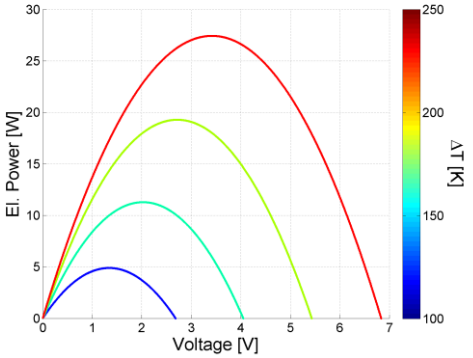

Figure 4. Electric power versus voltage for modules at different temperatures

Because of the linear relation between the voltage and current shown in Figure 3a, Figure 4 is very similar to Figure 3b. The same reasoning can, therefore, be applied here for a parallel case, i.e. modules connected in parallel operate at the same voltage, and one particular voltage corresponds to a maximum power output for only one temperature difference.

If connected modules are exposed to significantly different temperatures, sometimes the modules with a high temperature difference force the current to flow backwards in the modules with a low temperature difference. This implies that the low performing modules work as loads (Peltier coolers) to the high performing modules.

When designing a large TEG system for heat recovery from waste streams of liquids or gases, it is a very likely that the modules will operate under different thermal conditions since the energy content will be reduced substantially from the inlet to the outlet in the heat exchanger. This can partly be compensated for by gradually increasing the heat transfer from the fluid closer to the outlet. However, a simulation model must be able to take these non-ideal effects into account.

3 MEASUREMENTS

This research has involved several experimental studies. The measurement setups were built and measurements were performed both by the author and by partners in the industry, i.e. Volvo Technology AB and Termogen AB

3.1 MODULE MEASUREMENTS

Paper II describes a method for determining contact resistances inside a TE module based on module measurements and simulations. Paper III describes a framework for the characterization of modules and a generic model for a system of modules connected together that allows subgrid TEG models to be used with CFD simulation. The studies in both Paper II and Paper III required high accuracy measurements of temperatures, voltage, current, and heat flow in TE modules. The measurement setup was similar in the two studies, but the setup used in Paper III was expanded to allow for several modules to be measured at the same time in order to study a connected system.

The setup was based on commercial Bi_2Te_3 modules and solid aluminum blocks to achieve evenly distributed temperatures on the module surfaces. Each setup consisted of two modules that were located symmetrically around a heated block at the center. There were two water-cooled blocks on each side of the modules. On all sides of the modules, additional aluminum blocks were mounted to even out temperature as shown in Figure 5.

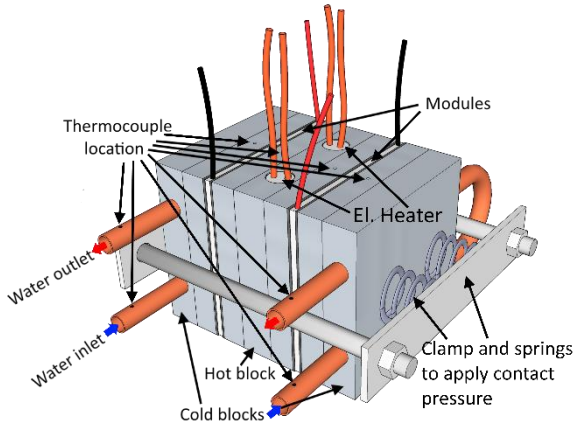

Figure 5. Schematic of measurement setup for module measurements

The temperatures were measured with thermocouples in the aluminum blocks. Several measurements were done at different locations in each block in order to confirm even distribution of temperature within the blocks. The TE modules were connected to an electronic load, LD300 from Thurlby Thandar Instruments Ltd. The inlet and the outlet temperatures on the cooling water were also measured together with the water mass flow rate to obtain the heat flow through the modules. The whole stack of blocks and modules were insulated to avoid heat losses to the surroundings. All temperature measurements together with the voltage over the modules were logged with DataTaker DT85 from Thermo Fisher Scientific Inc. Currents were measured by connecting low resistance (1mΩ) current shunts in series with the modules, and the voltage difference over them was also logged with the DT85 thus allowing the current to be calculated. The cooling water was fed in parallel to each cooling block from a tank maintained at constant temperature and a slight over pressure, and the mass flow rate of the water was controlled with valves at the outlet from the cooling blocks thus allowing accurate calibration of the flow rate.

The mass flow of cooling water was very stable with time and the uncertainty in the mass flow measurements was determined to approximately 0.2%. In order to determine the accuracy of the temperature measurements, the inlet and outlet temperatures of the cooling water were measured at steady state when the heaters were turned off. In these measurements, the difference between the inlet and the outlet temperatures was in the order of 0.05°C. Accordingly the uncertainty in

the heat flow measurements could be determined to a maximum of 1.17%, occurring at the measurement points with the lowest temperature differences.

The hot aluminum blocks at the center was heated with two electric heaters each. The electric heaters were controlled using a power regulator (Kemo Power Control M028N) to support a constant power to the heaters.

Measurements for studying the contact resistances described in Paper II were done with a load resistance that maximized the electrical power output from the modules at each thermal load point, i.e. where the load resistance matched the internal resistance of the modules. Measurements of the large modules described in Section 2.10 were used for determining the contact resistances, and measurements of the small modules were used for validation.

In Paper III, four of the large modules were studied, and the measurements showed some minor but not negligible differences between the individual modules. Two different sets of measurements were done for each of the four modules. The first set was measured at open circuit (no load connected) in order to measure the pure Seebeck voltage and thermal conduction through the modules. In this set of measurements, the power to the electrical heaters, and thereby, the temperatures was varied in several small steps, the measurements were done when the system reached thermal steady state. In the second set of measurements, the load resistance was varied from infinite (open circuit) to zero (closed circuit), and several measurements were sampled for each thermal load point at steady state. Repeated measurements were done to confirm repeatability. By first ramping up the current and then ramping it down, it was confirmed that no hysteresis existed. The measurements were first done to characterize the individual modules. Thereafter, the four modules were electrically connected together in a system working with one external load as shown in Figure 6.

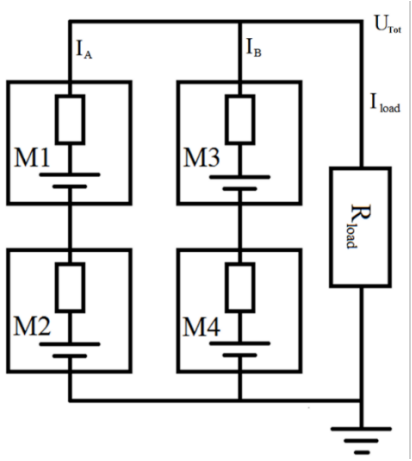

Figure 6. Schematics of the connected system used for validation.

In measurements of the connected system, the power to the electrical heaters was kept constant at different levels for the modules, and the load resistance was also varied from infinity to zero to allow a wide range of operating conditions to be studied.

3.2 HEAT PIPE PROTOTYPE

A technique for transporting relatively large amounts of thermal energy is to use the latent heat in phase shift materials. A heat pipe is a sealed pipe containing a mixture of vapor and liquid in which the transport is based on evaporation and condensation [52]. The pipe is kept vertical or possibly slightly tilted to the gravity field. The lower part of the pipe, containing the liquid, is heated and the liquid constantly evaporates. The vapor is transported with natural convection to the upper part of the pipe where it condenses, and thereby transfers its heat of evaporation. The condensed liquid is then transported downwards in the pipe by gravitational force. There are numerous different designs for heat pipes for different applications. However, the heat pipes used in this research were 12mm copper pipes with pure water as the working fluid. To increase the heat transfer area on the gas side, the lower part of the pipes was covered with copper fins on the outside. A full-scale prototype of an EGR cooler, based on these heat pipes for transporting heat from exhaust gas to the TE module surfaces, was built by Termogen AB.

The upper part of the heat pipes was connected to solid aluminum blocks, identical to the hot blocks used in the module measurements described earlier in Section 3.1. Two heat pipes were connected to each block, and one TE module was located on each side of the blocks. The modules used in this setup were the large modules described in Section 2.10. In addition to the hot blocks and the thermoelectric modules, the upper part of the prototype also consisted of cold aluminium blocks cooled with cooling water, similar to the setup for the module measurements in Section 3.1. A photo of the prototype and the corresponding CAD model can be seen in Figure 7. A total of 40 heat pipes, 20 hot blocks, 22 cold blocks, and 40 thermoelectric modules were used in the prototype. The prototype was tested in a single cylinder, 2.1 litre engine test rig at Volvo Technology AB, with the prototype located in the exhaust gas stream and not in the EGR circuit, for practical reasons. Mass flow rate, pressure drop, gas temperature at inlet and outlet, voltage and current were measured during all the experiments. The system of modules was connected to an electronic load (Amrel) where voltage and current was measured with an accuracy of 0.05%. The temperatures were measured with a temperature module, also with an accuracy of 0.05% (National Instruments, CT-120). Each test was run until stationary conditions were obtained.

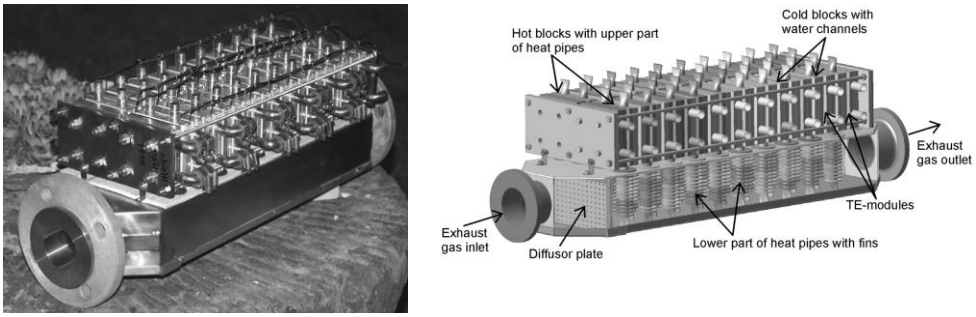

Figure 7. Heat pipe prototype a) Photo and b) CAD model.

As shown in Figure 7b, there was a diffuser plate located close to the inlet. The purpose of this plate was to distribute the gases evenly over the heat pipes, and, therefore, the holes were slightly larger along the sides to compensate for diverging flow sections at the inlet.

4 SIMULATION METHODOLOGIES

4.1 COMPUTATIONAL FLUID DYNAMICS

Computational fluid dynamics is a technique for solving the Partial Differential Equations (PDE) that describe a fluid flow numerically. The equations are based on two fundamental principles: the conservation of mass, and Newton's second law of motion. The law of the conservation of mass states that mass cannot be created nor destroyed. This is usually referred to as the continuity equation. Newton's second law of motion states that the time rate of change of momentum for a control volume plus the net change of momentum through the control volume is equal to the sum of all external forces acting upon the control volume. These are usually referred to as Navier Stoke's equations. Transport equations for energy, species, etc. can also be solved simultaneously.

In order to solve these equations, the computational domain must be divided into a computational grid, a so called mesh, and the PDEs are then discretized and solved using the Finite Volume Method (FVM). In this research, the commercial CFD software Ansys Fluent was used for solving the fluid flow and the heat transfer in the fluid. CFD can be used together with thermoelectric simulations in various ways. The main advantage of using CFD for analyses of TEG systems, is that spatial and temporal variations of heat fluxes and temperature distributions as well as the electric characteristics can be resolved simultaneously. This, however, requires additional models for thermoelectric generation, which will be discussed in Section 4.2

4.1.1 TURBULENCE MODELLING

In all CFD simulations involving turbulent flows, the turbulence must be solved for in order to achieve an accurate solution of momentum and heat flow. This can theoretically be done by solving the transient Navier-Stokes equations without simplifications, but this direct numerical solution (DNS) approach requires extreme computational power due to the wide range of time and length scales that must be solved for. In a real engineering application, this is never an option. Therefore numerous turbulence models have been developed based on the decomposition of the flow field in one average and one fluctuating part, an approach called Reynolds Average Navier Stokes (RANS) [53]. When rewriting the Navier Stokes equation using this decomposition, an additional term arises containing information about the exchange of momentum between the mean and the fluctuating parts of the flow field, and different turbulence models use different methods to describe this term, which is called the Reynolds stress tensor.

Two commonly used turbulence models in CFD are the k-ε and k-ω models. Both are two equation models which means that two additional transport equations are solved for the turbulence, i.e. the turbulent velocity, and the turbulent length scale. The difference between these models can be found in the transport equation describing the turbulent length scale. In the k-ε model, the transport equation describes the dissipation rate of turbulent energy ε, while in the k-ω model the specific dissipation ω, or turbulence frequency as it is also called, is described and used to determine the turbulent length scale [54].

In the boundary layers formed along walls, the turbulent kinetic energy and the turbulent length scale approach zero at the boundary. The k-ε model cannot be used in the boundary layer since it contains a term with the ratio of ε over k, and, therefore, both k and ε must approach zero at the correct rate in order for this term not to take extreme proportions.

When using the k-ε model or other high Reynolds models, special consideration must, therefore, be taken in the boundary layers. This can be done in different ways, e.g. by the use of algebraic wall functions instead of solving the governing equations in these regions. This method, however, requires a free stream with turbulent flow adjacent to the walls. In the event of narrow passages within the domain, where viscous forces are dominant, wall functions cannot be used. High resolution can, in these

cases, be achieved by solving the governing equations all the way to the wall, instead of wall functions, but dampening the source term of ε in low Reynolds regions. This approach is called low Reynolds modification or simply low Reynolds number turbulence models and a commonly used version is the Launder-Sharma turbulence model [55].

The k-ω, on the other hand, does not suffer from this shortcoming, and it can be used in the boundary layers, however, it requires a dense mesh in this regions and is more computationally demanding. Additionally, the boundary layer prediction in the k-ω model is very sensitive to the freestream values of ω and k [56].

The geometries studied in this work contain narrow passages, for example parallel fins, in order to increase heat transfer from the fluids. The dimensionless wall distance, y^+, in the middle between two fins is too low to allow wall functions to be used. In order to use wall functions, the first grid point must be in the lower part of the inertial sublayer, which is expected around $y^+ \sim 30$ [54]. The flow between the fins is influenced by viscous forces, and it is, therefore, not appropriate to use wall functions.

The SST k-ω model combines the advantages of the k-ω and k-ε models by applying the k-ω model in the boundary layers and the k-ε model in the bulk flow with a gradual transition. A very fine computational grid is, therefore, still required in the boundary layers for the SST k-ω model to give a correct result, i.e. y^+ values close to one are needed in the boundary layer, but the sensitivity of the free stream values of k and ω is avoided in this model by the advantage of freestream independence in the k-ε model. The SST k-ω model also contains other modifications making it suitable for a wider range of flow conditions, such as flows with adverse pressure gradients.

4.1.2 HEAT PIPE MODELLING

Analysis of the heat transfer through a heat pipe showed that this was not a limiting factor for heat transfer from the gas bulk to the hot block, instead the main transfer resistance was in the gas film. As a consequence, simulation of the heat flux inside the pipes can be simplified and the boiling condensation process does not need to be resolved. Instead the heat flux inside the pipes can be simulated

accurately using an effective heat conductivity. This approach reduces the complexity of the model significantly, and it was validated with measurements of the heat flow in single heat pipes for the temperatures relevant in the system. This strategy for modelling heat pipes has been presented earlier in the literature, and it was shown to give accurate results [57].

4.2 THERMOELECTRIC SIMULATIONS

The development of TE devices, such as thermoelectric generators and thermoelectric coolers (TEC) relies, to a large extent, on simulation tools for predicting thermoelectric performance. For this purpose, several studies have been conducted in order to evaluate the accuracy of the different modeling approaches proposed in the literature [58, 59]. The models proposed in the literature range from simplified macroscopic models based on the global balance of heat transfer and thermoelectric effects, to three-dimensional simulations based on the finite element method that accounts for all relevant thermoelectric phenomena, i.e. Seebeck, Peltier, Thomson, and Joule effects [60]. These so called first principle simulations solve the constitutive thermoelectric equations, Equations (2-13) and (2-14), in a computational grid created from the geometrical dimensions of the modules. First principle simulations are becoming widespread as they provide detailed information about potential, current flow, and temperature distribution inside the TE modules, and allow details in geometry and non-linear material properties to be accounted for easily. A thermoelectric toolbox based on FEM is included in the Ansys package, version 9.0 [60], and it has been used by several researchers for different applications [29, 58, 61].

One drawback of first principle simulations, however, is the large computational demand when these simulations are used for systems with many modules. Therefore, several simplified models of TE generators have been presented in the literature and Fraisse et al. have summarized some of the most common approaches and compared these to first principle simulations [59]. The models presented in this study were developed for TE legs, and they require temperature-dependent material data. They could in theory, after some additional development, be used to build subgrid models for CFD analysis, but that would require additional closures, such as thermal and electrical contact resistances.

These models would in a CFD analysis of a large system of modules, however, be quite computationally demanding since they require models for each individual TE leg.

Recently Montecucco and co-workers developed efficient models that can be used to simulate the electrical performance of large systems of modules working at different thermal loads when connected in series and in parallel [62]. These models do not provide any thermal characteristics, as is needed for a complete description of a TE generator, but their efficiency makes them interesting for further development. In Paper III, Montecucco's simplified model is further developed to include more physics, a novel model for heat flow is introduced, and a complete description of systems of TE models that is both accurate and efficient and at the same time allows for a two way coupling when implemented in a CFD analysis is presented.

A comparison between the different modelling strategies discussed above is summarized in Figure 8.

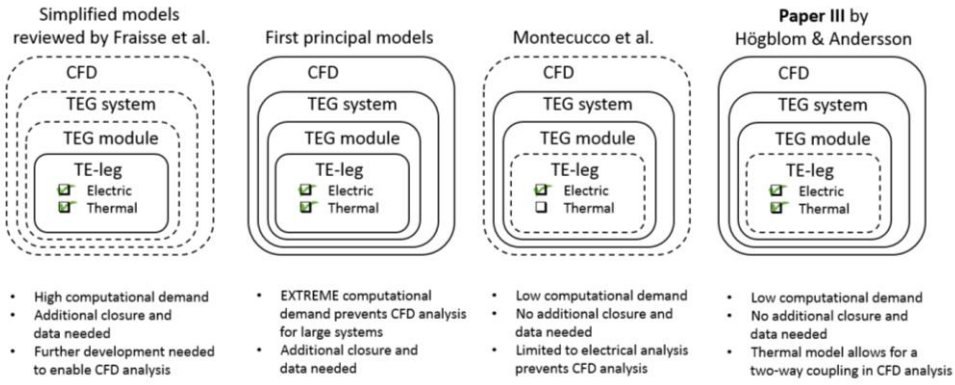

Figure 8. Comparison between the different modelling strategies.

Most applications for thermoelectric generators involve heat sources and/or heat sinks in which the energy is supplied by fluids. Therefore, it is of great importance to be able to simulate TEG systems together with fluid flows. Since the Peltier, Thomson, and Joule effects affect the temperatures of the surrounding fluids, a useful model must simultaneously predict thermoelectric and fluid dynamic behavior. This means that a two-way coupling in the energy equation is needed.

In a CFD analysis, a one-way coupling in the energy equation would mean that TE modules are simulated with an efficient heat conductivity to achieve temperature distribution. Thereafter, the thermoelectric generation would be solved for as a post processing operation. This approach effectively hinders the Peltier, Thomson, and Joule effects from being accounted for correctly since the generated current can never affect the temperature field. On the contrary, by using a two-way coupling in the energy equation, meaning the flow and temperature fields are solved simultaneously with the thermoelectric generation, the heat flow caused by the Peltier, Thomson, and Joule effects can be accounted for correctly.

In this thesis, the requirement of all TEG models used is that they should allow for this two-way coupling indicated by the outer the solid line in Figure 8. Therefore, the models used in this thesis are the first principle models and the subgrid model presented in Paper III.

4.2.1 FIRST PRINCIPLE MODELS

Two first principle models have been used in this research. In Paper I, a 3D thermoelectric model was built with user defined functions (UDF) in Ansys Fluent for the simultaneous prediction of fluid flow and thermoelectric generation. The equation that describes the potential field, Equation (2-13), was solved by rewriting it to a form that could be implemented as user defined scalars (UDS), which, for example, can be used to determine an electric field in a CFD environment. For each UDS implemented, one transport equation for that scalar is solved in Fluent [63]. The generic transport equation for a scalar ϕ_k is given by

$$\frac{\partial \rho \phi_k}{\partial t} + \frac{\partial}{\partial x_i}\left(\rho u_i \phi_k - \Gamma_k \frac{\partial \phi_k}{\partial x_i}\right) = S_{\phi_k} \tag{4-1}$$

where ρ is the density, u is the velocity, Γ_k is the diffusion coefficient and S is the source term.

Thermoelectric coupling into Ansys Fluent was implemented earlier by Chen et al. [26], and the approach in this research is similar.

This model was used in a simple geometry with only one thermocouple for simulation in steady state and in a transient condition with exhaust gases on one side in Paper I.

In Ansys Mechanical, there is a thermoelectric toolbox available [60] that solves the same equations, and this was used instead of the Fluent UDF model in Paper II. Ansys Mechanical uses a FEM solver instead of FVM as used in Ansys Fluent. It is theoretically possible to connect an unlimited number of thermocouples or TE modules in Ansys Mechanical. However, depending on the required mesh size and owing to limited possibilities for parallelization with FEM models, large models with several modules would be too computationally demanding to solve within a reasonable time even on a large computer cluster.

For Paper II, temperature-dependent material data for Bismut Telluride was obtained from the manufacturer of the modules [64], and the internal geometries of TE legs and electrical connectors inside the modules were measured with high accuracy.

In Ansys Mechanical, it is possible to define contact properties, such as thermal and electrical contact conductance between the different parts in the geometry. This allows the contact resistances to be determined based on a regression analysis of measured data of modules. Determining the contact resistances in this way was the objective in Paper II.

4.2.2 SUBGRID THERMOELECTRIC MODEL

When simulating real systems for thermoelectric generation consisting of several modules, the large number of internal parts that must be resolved, to fully account for the different thermoelectric phenomena, makes a first principle approach impractical and sometimes impossible even for computer clusters because of the high computational power this approach requires. This becomes even more apparent when the model is to be used in CFD analysis since it also requires resolution of the flow field, e.g. turbulent flow and local heat fluxes in the fluid domain, in addition to the resolution of individual modules. This problem can be overcome by developing simplified, efficient but accurate TEG models that can be used on a subgrid scale in CFD simulations.

In real applications, modules are usually electrically connected in series and/or parallel. If all connected modules do not operate at identical

temperatures, which is rarely the case, they will affect each other's electrical and thermal performance and cannot be controlled individually to operate at maximum power output. A useful subgrid TEG model must, therefore, account for this.

Paper III describes a framework in which such models are constructed based on regression analysis of measured data in terms of voltage, current, temperatures, and heat flow through TE modules. By using module measurements for finding the parameters in the models, both temperature-dependent material data and contact resistances are taken into account without any need for explicit measurements.

In order to develop a generic simulation framework that allows thermoelectric performance to be predicted efficiently, even for a large system of modules integrated into a heat exchanger, three different models are required, i.e. one electrical model and one thermal model for the individual modules and also one model for the connected system.

Paper III reports on the development of models for voltage and heat flow for individual modules. For predicting the electrical characteristics of individual modules, a reduced model with some modifications to extend the range of validity by imposing a more physical model was introduced in accordance with the work by Montecucco et al. [34].

To describe the total voltage over one module, the following model is proposed

$$U = U_{Seebeck}\left(\Delta T, T_{avg}\right) - I \cdot R_{int}(T_{avg}) \tag{4-2}$$

The first term is the Seebeck voltage, and the second term is the voltage drop caused by the current and the module's internal resistance.

To minimize the correlation between the parameters, two sets of measurement data were used for the regression; open circuit measurements to determine the Seebeck voltage that is independent of the current, and closed circuit measurements to determine the internal resistance. The regression polynomials used for the Seebeck voltage are given by

$$U_{Seebeck} = \left(\beta_{s1} + \beta_{s2} T_{avg}\right)\Delta T \tag{4-3}$$

where T_{avg} and ΔT are the average temperature and the temperature difference between the hot and the cold block, respectively. As seen in Equation (4-2), if the current is zero (open circuit), the voltage is given solely by the temperatures. If also the temperatures are the same on the different sides of the modules, i.e. $\Delta T = 0$, the Seebeck voltage is zero, as expected. Several alternative regression models for the Seebeck voltage are suggested in the literature that contain a constant term [62, 65], meaning that the model will predict a Seebeck voltage even at zero temperature difference, which is incorrect. These models can still be accurate within the operating range where the model is developed, but, since the physics has not been captured correctly, they will give poor predictions when extrapolated. In order to evaluate different polynomials for the Seebeck voltage, two sets of data found in the literature were used for comparison [66, 67].

When doing a regression analysis on this data, using different polynomials, the resulting R^2 values were found and are given in Table 1.

Table 1. Polynomials for Seebeck voltage with corresponding R^2 values

Polynomial	$(\beta_{s1} + \beta_{s2}T_{avg})\Delta T$	$\beta_s \Delta T$	$\beta_{s1} + \beta_{s2}\Delta T$
R^2 (Ashari et al.)	0.9983	0.9909	0.99732
R^2 (Hu et al.)	0.9994	0.96394	0.9987

As shown in Table 1, the proposed model, $(\beta_{s1} + \beta_{s2}T_{avg})\Delta T$, fits the literature data best. The next column shows the same model but without the term containing the average temperature, and this provides a less accurate description, shown by the lower R^2 value. The last column shows a model containing a constant term, such as the model in the work by Woo et al. [65] and Montecucco et al [62]. This model shows almost the same high R^2 values as the model proposed herein, but it is sensitive to extrapolation as it gives a non-zero voltage at zero temperature difference due to β_{s1}, as discussed earlier. In this case, the remaining voltage is -0.0369V and -0.2416V for the data by Ashari and Hu, respectively. In the papers by Montecucco et al. and Woo et al., the remaining Seebeck voltage at zero temperature difference is -0.96 and -

0.0056V, respectively. It can be noted that a relatively high R^2 value is achieved with the "one-parameter model" for the data by Ashari et al., which is explained by their measurements being done at only low temperature differences, meaning the temperature dependency of the material data was relatively constant in their study. Measurements were done at low temperature differences, which also is the reason that the predicted voltage by the model containing the constant term at zero temperature difference is very low. Also the model by Woo et al. was based on measurements at low temperature differences which explains the low remaining voltage at $\Delta T = 0$.

In addition to determining parameters that describe the Seebeck voltage, the data set measured with a closed circuit and varying load resistance was used to determine parameters that describe the module's internal resistance.

The model for the Seebeck voltage was used to calculate the Seebeck voltage for every point in the data set with varying load resistance (closed circuit). Since the current was also measured, the internal resistance in the module could be determined from Equation (4-2), i.e.

$$R_{int} = \frac{(U_{Seebeck} - U)}{I} \tag{4-4}$$

and since the internal resistance is a function of the absolute temperature in the module, which has a temperature dependency, it was modelled as

$$R_{int} = \beta_{R1} + \beta_{R2} T_{avg} + \beta_{R3} T_{avg}^2 \tag{4-5}$$

The resulting model for the voltage can be summarized as

$$U = \left(\beta_{s1} + \beta_{s2} T_{avg}\right)\Delta T - I\left(\beta_{R1} + \beta_{R2} T_{avg} + \beta_{R3} T_{avg}^2\right) \tag{4-6}$$

A model for the heat flow was developed using a similar methodology that allowed the heat flow to be determined as a function of temperatures and current. The suggested model for the heat flow on the cold side is

$$Q_c = Q_{cond}(\Delta T, T_{avg}) + I \cdot \Psi_{Pelt+Thom,cold}(\Delta T, T_c, T_{avg}) + \frac{I^2 \mathrm{R}_{int}(T_{avg})}{2} \quad (4\text{-}7)$$

The first term in Equation (4-7) is the conduction that is independent of the current through the module, the second term is the Peltier and Thomson effects combined, and the last term is the Joule heating. The measurements on open circuit were used to determine the conduction term since this is the only effect that occurs when no current is allowed to flow.

A similar expression to the Seebeck voltage was used for the Fourier conduction in order to take the temperature dependency of the thermal conductivity into account and also ensure a vanishing conductive heat flow at zero temperature difference.

$$Q_{cond} = (\beta_{F1} + \beta_{F2} T_{avg})\Delta T \quad (4\text{-}8)$$

Since the internal resistance is calculated in the voltage model, it can be used directly to determine the Joule heating term, and the heat flow measurements can thus be used to determine the Peltier and Thomson effects.

$$\Psi_{Pelt+Thom,cold} = \frac{Q_c - Q_{cond}}{I} - \frac{I \mathrm{R}_{int}}{2} \quad (4\text{-}9)$$

For thermoelectric material, the Thomson coefficient, τ, can be expressed by the Kelvin relation as the derivative of the Seebeck coefficient with respect to temperature times the absolute temperature, $\tau = \partial\alpha/\partial T \cdot T$. Furthermore, the Thomson effect is the Thomson coefficient times the current density and the temperature gradient, $\mathrm{q}_{Thomson} = \tau J \nabla T$. When combining these equations, a quadratic dependency on the temperatures is apparent ($T_{avg}\Delta T$). Additionally, the Kelvin relation that describes the Peltier coefficient is the Seebeck coefficient times the absolute temperature, $\Pi_{Peltier} = \alpha T$, which allows a model for the combined Peltier and Thomson effect to be written

$$\Psi_{Peltier+Thomson,cold} = \beta_{PT1}T_c + \beta_{PT2}T_{avg}\Delta T \tag{4-10}$$

The resulting model for the heat flow is given by

$$Q_c = \left(\beta_{F1} + \beta_{F2}T_{avg}\right)\Delta T + I\left(\beta_{PT1}T_c + \beta_{PT2}T_{avg}\Delta T\right) + \frac{I^2\left(\beta_{R1} + \beta_{R2}T_{avg} + \beta_{R3}T_{avg}^2\right)}{2} \tag{4-11}$$

Equation (4-11) describes the heat flow on the cold side of the module. At steady state, the heat flow entering the module on the hot side is the same but with one additional term that describes the heat flow converted to electric energy,

$$P_{el} = IU = I\left(\beta_{s1} + \beta_{s2}T_{avg}\right)\Delta T - I^2\left(\beta_{R1} + \beta_{R2}T_{avg} + \beta_{R3}T_{avg}^2\right) \tag{4-12}$$

When this is inserted in Equation (4-11), the heat flow on the hot side can be expressed as

$$Q_h = \left(\beta_{F1} + \beta_{F2}T_{avg}\right)\Delta T + I\left(\beta_{PT1}T_c + \beta_{PT2}T_{avg}\Delta T\right) + I\left(\beta_{s1} + \beta_{s2}T_{avg}\right)\Delta T - \frac{I^2\left(\beta_{R1} + \beta_{R2}T_{avg} + \beta_{R3}T_{avg}^2\right)}{2} \tag{4-13}$$

It should be noted that the Peltier Thomson term on the hot side is the sum of the second and the third terms in Equation (4-13), i.e. $\mathrm{Q}_{Peltier+Thomson,hot} = \mathrm{Q}_{Peltier+Thomson,cold} + IU_{Seebeck}$.

Finally a model for the connected system is needed to provide a closed set of equations that can be solved implicitly.

This is straightforward and can be done for any electrical configuration using Ohms law and Kirchhoff's laws. In order to propose a general

model that could be implemented in a subgrid CFD model, a system of *m* serial connected groups, each containing *n* modules, was studied. A schematic diagram of the general system is shown in Figure 9.

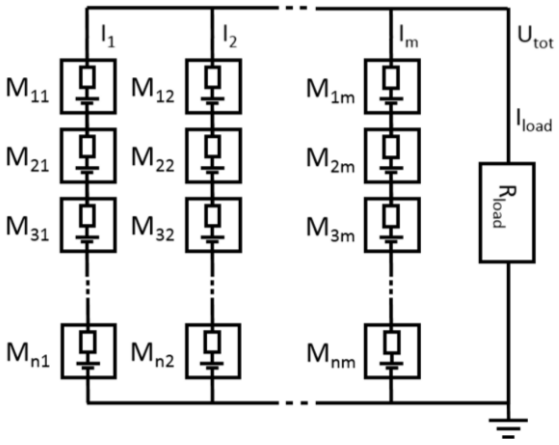

Figure 9. Schematics of general system with $\boldsymbol{n \cdot m}$ modules.

The total voltage over the load, U_{tot} is given by the sum of voltages in any of the serial connected groups, according to Kirchhoff's voltage law

$$U_{tot} = \sum_{j=1}^{n} U_{ji} \qquad \forall\, i \in \{1, \dots, m\} \tag{4-14}$$

where the voltage over each module, U_{ji}, is the Seebeck voltage minus the Ohmic voltage drop according to Equation (4-6), which for the generic system is formulated as

$$U_{ji} = U_{seebeck,ji} - I_i R_{ji} \qquad \forall\, i \in \{1, \dots, m\}, j \in \{1, \dots, n\} \tag{4-15}$$

The load current, I_{load}, can be expressed by Ohm's law, and it is given by

$$I_{load} = U_{tot} / R_{load} \tag{4-16}$$

The load current is also equal to the sum of current in the different groups according to Kirchhoff's current law

$$I_{load} = \sum_{i=1}^{m} I_i \tag{4-17}$$

Given a temperature difference, $U_{seebeck,j,i}$ and R_{ji} can be calculated for each module since they are independent of the current. The equation system consisting of Equations (4-14) – (4-17) can then be solved in an iterative manner. This is under the assumption that the load resistance, R_{load}, is known.

In order to maximize the electrical power output, the load resistance should match the resistance in the connected system of modules, i.e. it can be calculated as

$$R_{load} = \frac{1}{\sum_{i=1}^{m} \left(\frac{1}{\sum_{j=1}^{n} R_{ji}} \right)} \tag{4-18}$$

Since none of the currents in the groups (I_1 ... I_m) are known, (in general) these equations have to be solved in an iterative manner. Knowledge of the current through the different groups allows the heat flows to be determined by Equations (4-11) and (4-13).

4.2.3 STATISTICAL EVALUATION

In this thesis, different models have been developed by use of regression analysis. To evaluate the accuracy of the models, the coefficient of determination, R^2, is used. It is a statistical measure of how well a model fits experimental data, and it is defined as the ratio of the variance explained by the model to the total variance in the measurements. Adjusted R^2 is a modification of R^2 in which the number of explanatory variables are taken into account. A comparison between the R^2 and adjusted R^2 is thereby a measure of whether the model is over parametrized [68].

When a regression model in used on a set of data that is not used for the regression analysis to determine the model parameters, R^2 can be calculated, and it then becomes a measure of how well the model predicts the new data. To distinguish this measure from R^2 based on the data used for regression, it is in this thesis referred to as "Model R^2". All statistical analysis were done using Matlab.

5 RESULTS AND DISCUSSION

In this work, simulations of thermoelectric generators have been carried out from two different approaches. In Paper I, the in-house code for the thermoelectric effects described in Section 4.2.1 was used. In this model, the first principle equations, Equations (2-13) and (2-14) are solved directly by the solver in Fluent.

Also in Paper II, a simulation strategy based on solving these first principle equations was adopted, but, in this study, the thermoelectric toolbox in Ansys Mechanical was used. A different approach was used in Paper III and Paper IV, in which models for TEG modules are proposed and coefficients are determined based on measurements of module performance under varying conditions.

5.1 FIRST PRINCIPLE SIMULATIONS (PAPER I & II)

5.1.1 TRANSIENT OPERATION

The first study presented in Paper I, relies on a single thermocouple in conjunction with a small gas domain simulated using Ansys Fluent with the UDF model. Both steady state and transient simulations were conducted.

The steady state simulations were done in order to study the temperature distribution from the hot exhaust gas to the cold side of the thermocouple. In the transient simulations, measurements of temperature variations in the exhaust gases during a vehicle test cycle, see Figure 10, were used in order to determine whether or not it is advantageous to smooth temperature fluctuations or to use high peak temperatures.

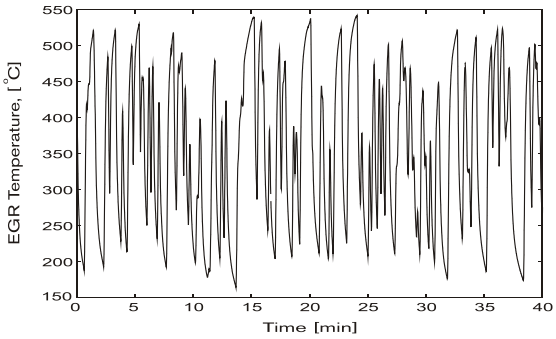

Figure 10. Transient temperatures in the EGR cooler inlet from a vehicle test cycle.

A representative one-minute long sequence of the test cycle was chosen for the simulations, and the hot gas temperatures were changed in accordance.

The simulated geometry consisted of one thermoelectric pair connected with copper plates and a small channel that allowed a flow of exhaust gases parallel to the hot copper plate.

Measurement data from $Ba_8Ga_{16}Ge_{30,}$ developed within E4-Mistra, was used in the simulations [69].

The results from the steady state analysis clearly showed that it is essential to reduce the heat transfer resistance in the gas in order to achieve a large temperature difference over the thermoelectric elements. As can be seen in Figure 11, about 1/3 of the temperature drop was located in the gas, which corresponds to approximately a loss of 33% of the potential power output.

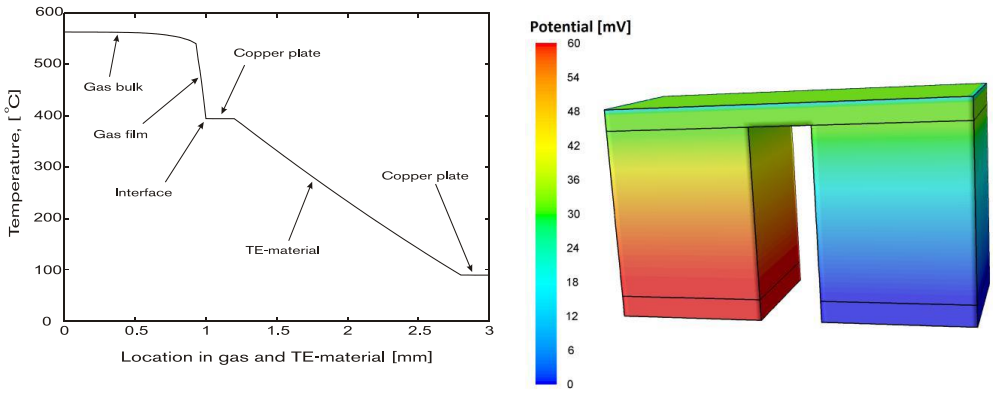

Figure 11. a) Temperature distribution across the channel and TE material and b) Total potential in thermocouple.

Transient simulations were used to predict power generation as a function of time during the reduced vehicle cycle. The sequence chosen from the driving cycle is shown in Figure 12a. Both the temperature in the exhaust gas manifold and the partly smoothed temperatures in the EGR cooler were simulated and compared to their averages. The resulting power output from the thermocouple in all four cases is shown in Figure 12b.

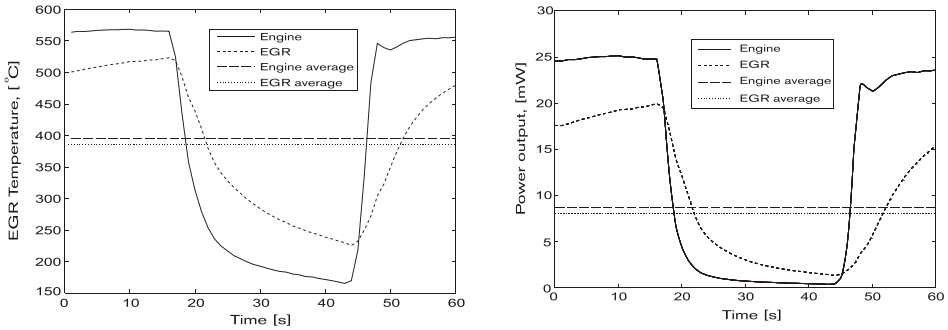

Figure 12. a) Temperatures in exhaust gas manifold and EGR during a reduced vehicle cycle. b) Power output from one thermocouple simulated at 66% of ΔTmax.

The power output was integrated with respect to time in order to achieve the energy delivered by the thermocouple during this reduced vehicle cycle. The result is summarized in

Table **2**. As can be seen, higher performance was achieved when transient data with temperature fluctuations was used instead of average temperatures. These results strongly depend on the TE material used and the temperature dependence of the *ZT* of the material.

Table 2. Energy comparison over a reduced vehicle cycle.

Analysis	**E [J]**	**$E_{transient}$ / $E_{average}$ [-]**
Engine, transient temperature	0.78	1.5
Engine, average temperature	0.52	
EGR, transient temperature	0.58	1.21
EGR, average temperature	0.48	

5.1.2 CONTACT RESISTANCES

In the second study presented in Paper II, the thermal and electrical contact resistances inside a TE module were determined from the measurement data of temperatures, voltage, current, and heat flow through a module. The experimental setup is further described in Section 3.1. A simulation model of the TE module was built in Ansys Mechanical, Figure 13. Temperature-dependent material data was used inside the TE pellets. Contact resistances were implemented at the interfaces inside the module, and these were varied in order to minimize a normalized sum of square errors with a steepest gradient method. All the thermal resistances inside the module and on its surfaces were grouped together into two different parameters in the model, one on the hot and one on the cold side. The electrical contact resistance was assumed to be identical at all material junctions. This assumption is acceptable since it is the sum of all resistances that is important for a correct description of the electric output.

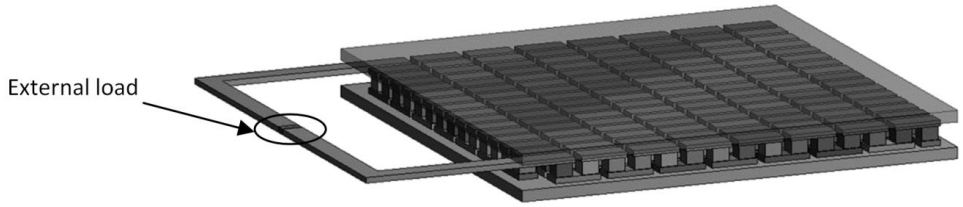

Figure 13. Simulation model of the thermoelectric module.

A comparison between measurements and simulations with and without contact resistances is shown in Figure 14. As shown, there are major deviations between measurements and simulations if contact resistances are not included in the models, despite correct material data and accurate measurements of the internal component sizes and arrangement.

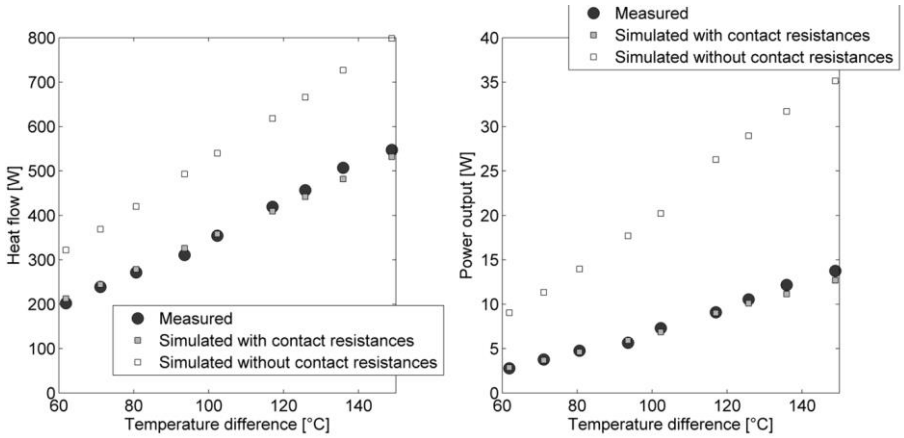

Figure 14. Comparison of measurements and simulations with and without contact resistances from TEHP1-12680-0.15 (80x80mm) a) heat flow, and b) electric power output.

Simulations with different contact resistances on the internal interfaces described in Section 2.11 were carried out for the same modules, and a regression analysis was performed in which the normalized sum of square errors for heat flow, current, and voltage was minimized, i.e.

$$\min_{r_h, r_c, \varrho} \left(\sum_{i=1}^{n} \left(\frac{U_i - \hat{U}_i}{U_i} \right)^2 + \sum_{i=1}^{n} \left(\frac{I_i - \hat{I}_i}{I_i} \right)^2 + \sum_{i=1}^{n} \left(\frac{Q_i - \hat{Q}_i}{Q_i} \right)^2 \right) \quad (5\text{-}1)$$

The simulation results achieved with the determined contact resistances in terms of heat flow and delivered electrical power can also be seen in Figure 14.

The thermal contact resistances within the modules were found to be $r_h = 2.0 \cdot 10^{-4}\ m^2KW^{-1}$ on the hot side and $r_c = 1.0 \cdot 10^{-4}\ m^2KW^{-1}$ on the cold side. The electrical contact resistance for the studied modules was determined to be $\varrho = 4.8 \cdot 10^{-9}\ \Omega m^2$.

Both the thermal and the electrical contact resistances were found to be in the range reported in the literature [29]. They are significant in comparison with the resistances offered by the bulk material.

The R^2 statistics and the adjusted R^2 are statistical measures of how much of the total variance in the experiments can be explained by the model. This is further described in Section 4.2.3. R^2 statistics and adjusted R^2 values are given in Table 3

Table 3. R^2 values for the three response variables for TEHP1-12680-0.15.

	R^2 statistics	Adjusted R^2
Heat flow	98.3%	98.1%
Current	97.5%	97.2%
Voltage	98.7%	98.5%

The contact resistances determined in the regression analysis for the large modules were used in simulations of small modules. This was done to determine whether or not these resistances are general for these kinds of modules made with the same materials and with the same process parameters. The simulated and measured values of heat flow, current, and voltage can be seen in Figure 15.

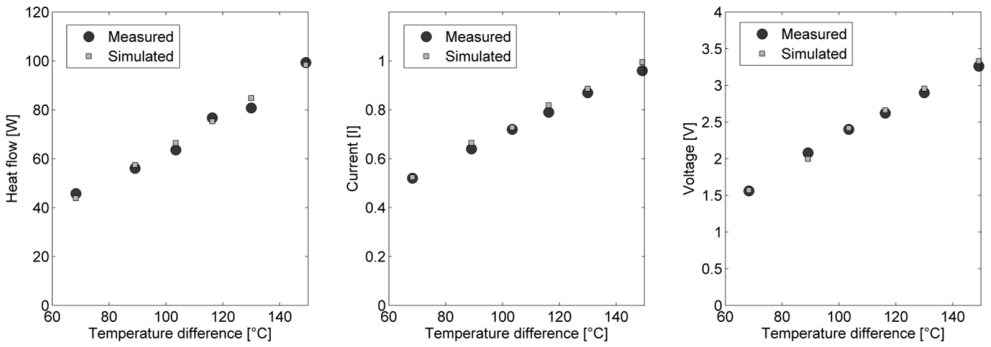

Figure 15. Simulated and measured values for TEP1-1264-1.5 a) heat flow, b) current, and c) voltage.

As can be seen, there is almost perfect agreement between measured and simulated data for these modules, as well. The corresponding R^2 values are given in Table 4.

Table 4. Model coefficient of determination for the three response variables for TEP1-1264-1.5.

	Model R^2
Heat flow	97.4%
Current	97.8%
Voltage	98.7%

These values are only slightly lower than the values for the large module and confirm that the model is capable of predicting module performance very well. There is no lack of fit in the model, i.e. there are no systematic deviations between simulated and measured values of voltage, current, and heat flow over the entire operating range. If no contact resistances had been included in the simulations, then voltage, current and heat flow would also have been significantly over-predicted for this module.

5.2 MULTI-SCALE SIMULATIONS (PAPER III & IV)

In order to do CFD simulations of large TEG systems, an efficient and accurate subgrid TEG model was developed and presented in Paper III. In Paper IV, this model is implemented in the heat pipe prototype described in Section 3.2, and the simulation results are compared with measurements.

5.2.1 MULTISCALE MODEL

A comparison between measured and simulated electrical power and heat flow for a single module is shown in Figure 16. The color scale is used to visualize the temperature difference the modules operate at.

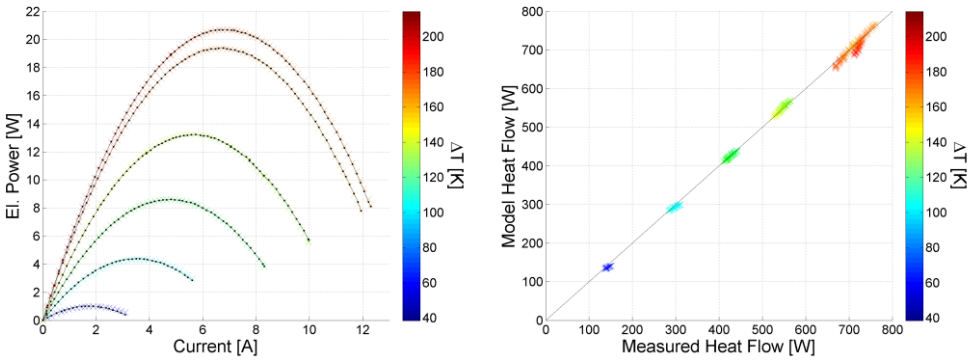

Figure 16. a) Measurements (colored according to ΔT and simulations (black) of electric power from a module versus current. b) Modeled heat flow versus measured heat flow colored according to ΔT

As can be seen in Figure 16, the model fits the experimental data very well throughout the whole measured temperature and current range.

The R^2 for the voltage and heat flow of the suggested model is summarized in Table 5 together with the corresponding adjusted R^2 and both confirm very good agreement between measurements and models.

Table 5. Coefficient of determination, R^2.

	Voltage		Heat flow	
	R^2	R^2 adj	R^2	R^2 adj
Module 1	0.9995	0.9995	0.9956	0.9955
Module 2	0.9990	0.9990	0.9980	0.9980
Module 3	0.9991	0.9991	0.9965	0.9964
Module 4	0.9998	0.9998	0.9979	0.9979

These high R^2 values show that the model is able to predict thermal and electrical performance very well. The similar values of R^2 adjusted indicate that the model is far from over parametrized, and additional parameters could potentially be included in the model. It is, however, hard to physically motivate additional terms in the models, and even if higher order polynomials would result in higher R^2 values, the drawback would be a higher correlation between the parameters, which would lower the accuracy when the model is extrapolated outside the operating range used for determining the regression parameters. The physical formulation of the model is important in that it allows the model to be used far outside the measured operating range, i.e. when the current is reversed and the modules operate as Peltier coolers rather than generators.

When modules in the connected system described in Section 3.1 were exposed to different temperatures, the current generated by the modules exposed to a high temperature difference forced the modules operating at a low temperature difference to work with a reversed current and, thereby, operate as Peltier coolers. This allowed the model to be validated when extrapolated to extreme conditions, i.e. where it was not possible to obtain data for individual modules with the current setup.

Figure 17a shows the electrical power output of the different modules as a function of the current through the load. The corresponding modelled heat flow through the modules versus the measured heat flow is shown

in Figure 17b. The same color scale as in Figure 16 is used to visualize the module's temperature difference.

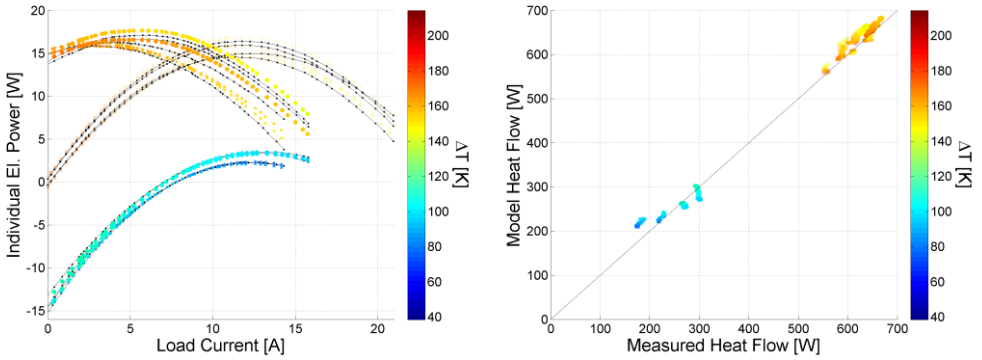

Figure 17. a) Measurements (colored according to ΔT) and simulations (black) of electric power from individual modules versus load current. b) Modelled heat flow versus measured heat flow, colored according to ΔT

When the modules operate with different temperature differences, it is obvious that the modules sometimes have a negative contribution to the system's total electrical power output. Obviously, when there is no current through the load, no useful power is being generated. At this point, all electric current generated in the high performing modules is consumed in the low performing modules, where it pumps heat from the cold to the hot side with the Peltier effect.

It is concluded that the simulation framework presented in Paper III allows very good prediction of both thermal and electrical performance for a wide range of operating conditions. A statistical evaluation of the entire data set shows that the model allows 99.6% and 99.9% of the variance in voltage and current, respectively, and 97.4% of all variance in the heat flow to be predicted, as summarized in Table 6.

Table 6. Model R^2 determined for the connected system.

	Module 1	Module 2	Module 3	Module 4
Voltage	0.99562	0.99676	0.99818	0.99694
Current	0.99959	0.99959	0.99962	0.99962
Heat flow	0.99205	0.99505	0.99287	0.97446

As shown in Table 6, the model R^2 values for the current are identical for modules 1 and 2 as well as for modules 3 and 4. This is expected since they are connected in series, and the current through them, thereby, is the same.

If measurements with reversed current should be done for individual models working under these conditions, the external load can be changed to a DC power supply, allowing different operating points with reversed currents to be measured. By adopting this minor modification to the experimental setup, the framework described in Paper III could be used to measure modules primarily intended for Peltier cooling, a similar extrapolation to modules operating as generators could then be used for validation. This could also be done to extend the range of validity for the model, but, as shown here, this should not be necessary since the model predicts performance very accurately even outside the measured operating range.

5.2.2 CONCEPTUAL STUDIES OF CONNECTED SYSTEMS

When modules experiencing different temperatures are connected electrically to one single load, the voltage and/or current cannot be controlled individually in the modules to achieve optimal power output. Since combinations of serial and parallel connections are frequently used to control the voltage level in larger systems of modules, it is important to understand and be able to predict these effects. At the same time, it is important to understand and predict the heat flow in these systems. By using the validated model presented in Paper III, two basic configurations were studied to further investigate the different phenomena that contribute to the total heat flow and to investigate the importance of a two-way coupling of energy, when the models are implemented in CFD analysis.

In the first configuration, two modules were connected together electrically in series, Figure 18a, and the second configuration consisted of modules connected in parallel, Figure 18b. The heat conduction, Peltier and Thomson effects, and Joule heating were studied separately when the modules operated at different temperatures.

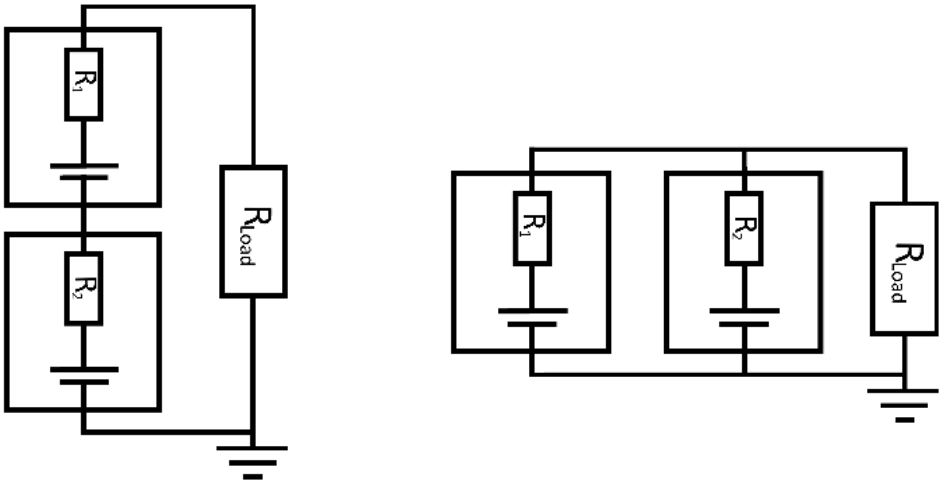

Figure 18. Schematics for simulation of two modules in a) serial and b) parallel configurations

The temperature differences in each module ranged from 0°C to 270°C. At all the simulated points, the load resistance was chosen to achieve a maximal power output from the system, i.e. it was chosen to be the same as the internal resistance in the connected system at given temperatures. The internal resistance in the modules was first calculated for the individual modules at given temperatures from the models developed earlier and then combined to give the total resistance according to Equation (4-18), i.e. $R_{serial} = R_1 + R_2$, and $R_{parallel} = 1/(1/R_1 + 1/R_2)$. For each combination of temperatures in the two modules, the current was determined by solving Equations (4-14) – (4-17) in an iterative manner. The current through module 1 as a function of the temperature differences over that module (ΔT_1) and the temperature difference over the other second module (ΔT_2) for both the serial and the parallel configurations are shown in Figure 19.

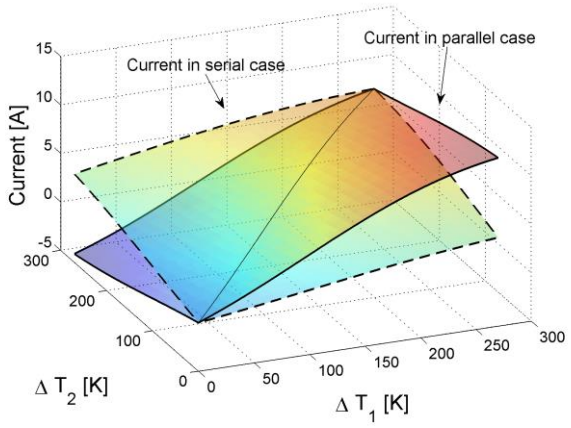

Figure 19. Current through module 1 for serial and parallel configuration versus temperature differences.

As could be expected, the current was always positive when the modules were connected in series but was sometimes negative for some combinations of temperatures for modules connected in parallel. When both modules operated at the same temperature, the current through them was the same for both the serial and parallel cases, see diagonal in Figure 19. This can be explained by the fact that, since the load resistance was chosen to maximize the total power output, both modules independently worked at their maximal power output and, therefore, did not affect each other's voltage or current.

Figure 20a shows the heat flow on the cold side generated by the Peltier and Thomson effects and also the total Joule effect in module 1 as a function of ΔT_1 and ΔT_2 for the serial connected modules. Figure 20b is the corresponding plot for the parallel connected modules.

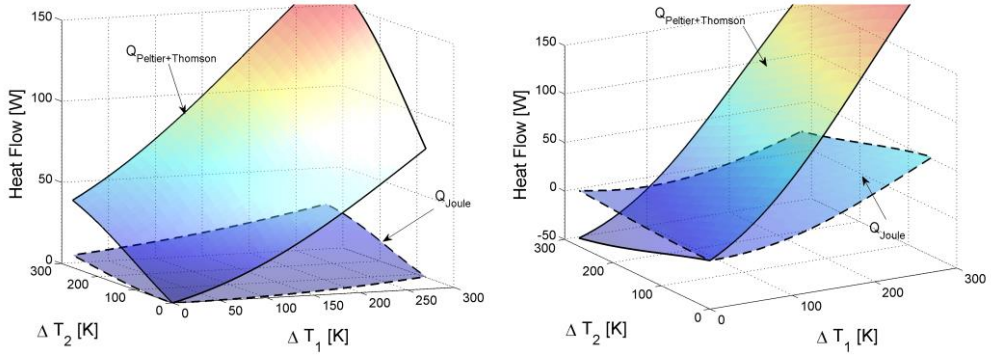

Figure 20. Peltier, Thomson and Joule effects in module 1 as a function of ΔT_1 and ΔT_2 in a) serial and b) parallel configurations.

In Figure 20, the uppermost surface in each plot is the Peltier and Thomson effects. The lower surface is the Joule effect. Naturally the shape of the Peltier and Thomson effects follow the shape of the current surface plot shown in Figure 19 since they have a proportional relationship. When the current through the module in some areas in the parallel configuration is negative, so will the Peltier and Thomson effects be as can be seen to the left in Figure 20b. The Joule heating also follows the current, but it never becomes negative and instead increases for negative currents since it contains the square of the current. In other words, reversing the current still heats the module with the Joule effect.

As shown in Figure 20a and b, the Peltier and Thomson effects increase with the temperature difference in module 1, ΔT_1, when the temperature in module 2, ΔT_2, is kept at zero temperature difference for both the serial and parallel configurations. In this case, module 2 works as an extra load (increasing or decreasing the total load for the serial and the parallel configurations, respectively) that affects the current through the module and, thereby, the magnitude of the effects. When ΔT_1 was kept constant and ΔT_2 increased in the serial configuration, module 2 drove a larger current through both modules, thereby increasing the Peltier and Thomson as well as the Joule effects. In the parallel configuration, the increase in temperature difference, ΔT_2, resulted in a larger current in module 2, and since the sum of the current through the modules must equal the load current, the current through module 1 decreased, and,

thereby, the Peltier, Thomson, and Joule effects also decreased in module 1.

Figure 21 shows the pure heat conduction for the same conditions. The conduction is only a function of the temperatures and not of the current, which means it is independent of the other module.

If CFD simulations of a TEG system are performed with a one-way coupling approach for the energy equation, only the conductive heat flow will be solved for. Comparing Figure 20 and Figure 21, it can be seen that the magnitude of the Peltier and Thomson effects are, as can be expected, in the order of approximately 10-20% of the heat conduction. The Joule heating had a much smaller but still non-negligible contribution. In a large system with several modules, the current might increase even more and, thereby, also these current-dependent thermal effects. Using a one-way coupling results in that none of these phenomena would be fed back to the fluid flow with noticeable errors in the energy equation. Since the Peltier, Thomson, and Joule effects change the temperatures on the TEG surfaces, the prediction of voltage and current will also be affected unless a two-way coupling is implemented.

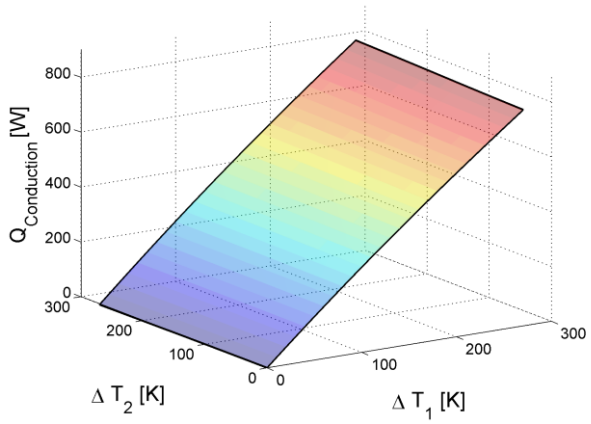

Figure 21. Thermal conduction through module 1 as function of ΔT_1 and ΔT_2.

5.2.3 HEAT EXCHANGER PROTOTYPE SIMULATIONS

In Paper IV, the subgrid models developed in Paper III were implemented in a CFD analysis of the heat pipe prototype described in Section 3.2. Experiments were done in an engine bench at different engine loads,

allowing predictions under different hydrodynamic conditions, turbulence intensity, and exhaust gas temperatures. Three different engine loads were simulated and compared with experiments and these provided a validation of the complete multiphysics multiscale model. In the experiments, engine speed, torque and fuel injection were varied resulting in different thermal flows in the heat exchanger. The load points were chosen in order to span a large operating range, i.e. low, moderate, and high thermal loads. A comparison between measurement and simulation results is shown in Figure 22.

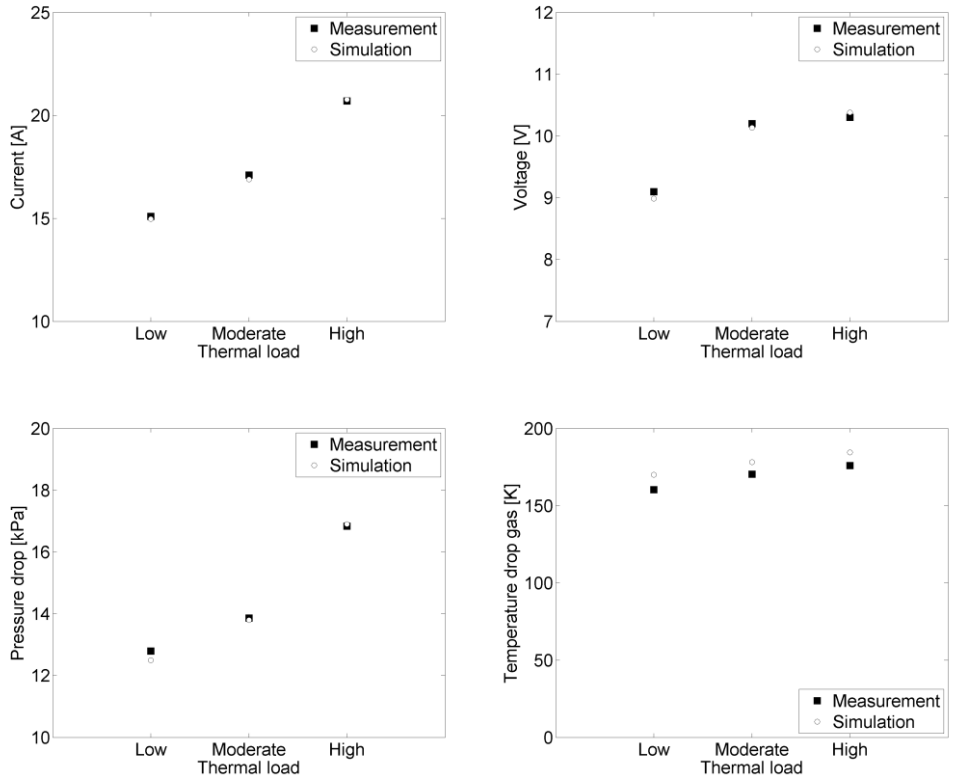

Figure 22. Comparison between experiments and coupled CFD and TE simulations, a) Current, b) Voltage, c) Pressure drop, and d) Gas temperature drop.

In general, the simulation agrees very well with measurements. In terms of current, voltage, and pressure drop over the system, the agreement is excellent. The temperature drop of the exhaust gases from the inlet to the outlet shows a slightly larger difference between measurements and

simulations, ≤ 6% which is still acceptable. A possible reason for this deviation can be found when studying the temperature distribution over the outlet. Figure 23 shows the temperature field in a horizontal plane overlayed with streamlines coloured according to residence time.

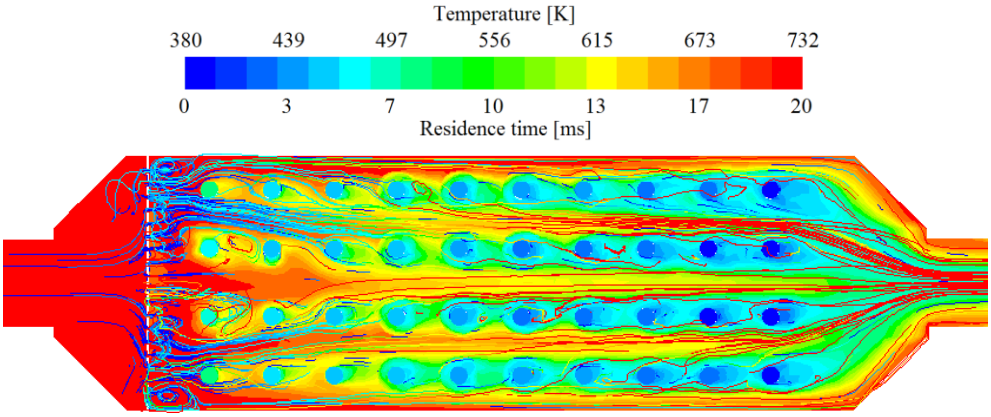

Figure 23. Temperature distribution and streamlines in a horizontal plane for the simulation at moderate thermal load.

From Figure 23, it is clear there is a large temperature difference over the outlet which makes temperature measurements sensitive to the location of the thermocouple. In this simulation, the difference between the centre and the walls is as high as 150°C, which can explain the small but systematic differences between measurements and simulations seen in Figure 22d.

Figure 24 shows the surface temperature of the heat pipes and the aluminium blocks.

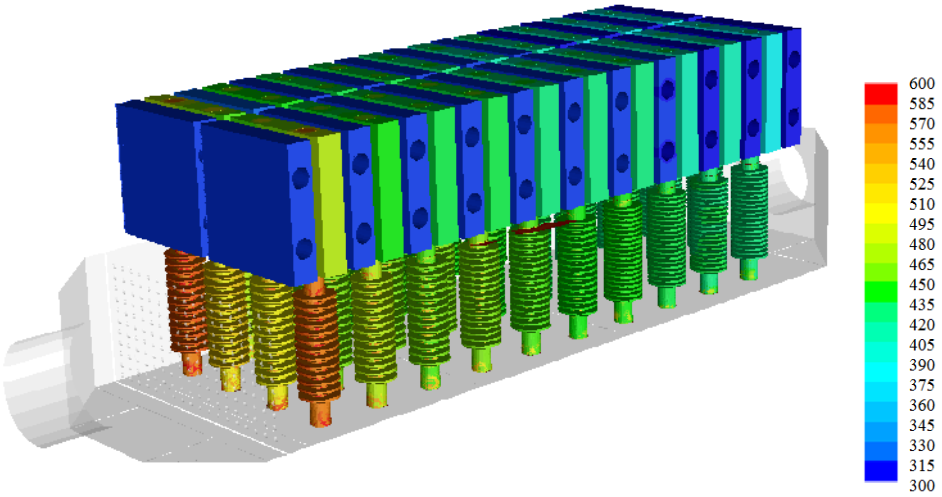

Figure 24. Temperature distributions of heat pipes and aluminum blocks for the high thermal load case.

The diffusor plate close to the inlet was designed with larger holes close to the sides and smaller holes in the middle. This was done in order to distribute the flow evenly to all the heat pipes. The higher temperature of the outermost heat pipes in the first row is a consequence of this design, i.e. the hole pattern actually over compensated and resulted in a larger flow and, thereby, a larger heat transfer to the outermost pipes. It is also clear in the figure that the temperature of the heat pipes and modules decreases along the heat exchanger despite the attempt to compensate for the lower temperatures in the gases by increasing the fin density along the flow direction. As mentioned earlier, this has a negative impact on the total electrical power output of the system since the modules are connected electrically. To get an estimate of the magnitude of these non-ideal effects, and, consequently, the error that is introduced if a simplified TEG model is used that does not contain take the electrical connection in the system into account, the module surface temperatures obtained in the simulations were used to simulate all modules in a fictive case in which all modules operated individually with optimal current.

In the three load cases studied, these optimal simulations resulted in an over prediction of the electrical power output of 5.4%, 5.2%, and 4.6%, in the high, moderate, and low load case respectively.

All these results show that the prototype is far from optimized, but it still serves the purpose of validating the multiphysics model. From the comparisons between simulation results and measurement data, it is concluded that by using these multiphysics simulations, reliable prediction of pressure drop, heat transfer, and thermoelectric power generation can be achieved. The non-ideal effects seen here might be avoided and the whole design can be improved if these simulation tools are used prior to building prototypes.

The non-optimized design of the prototype also results in that just a small part of the available energy in the exhaust gases is transferred. In all three cases it was around 35%, which can be compared with the goal of around 60-70% that is targeted if used in an EGR cooler [70]. A larger amount of energy extracted from the gases would result in a larger gas temperature drop from inlet to outlet, and if the design does not compensate enough with a larger heat transfer downstream, the modules will be exposed to increasing temperature differences resulting in larger non-ideal effects.

In order to understand how such a design would perform in terms of generated thermoelectric power, and quantify the non-ideal effects, an analysis with increased heat transfer in the gas were performed. This simulation was done for the case with a low thermal load in order not to exceed the maximum temperature that modules can withstand in the heat exchanger. The results are summarized in Table 7.

Table 7. Comparison between real and optimal power output at different heat transfer efficiencies and temperature profiles.

Transferred energy [%]	Real power [W]	Optimal power [W]	Difference [%]
34%	136.2	142.5	4.6
56%	335.8	379.6	13.0

As can be seen, the difference between the optimal electrical power and the real power in a connected system of modules increases significantly with the amount of energy extracted from the gases. This is a direct result

of the larger temperature differences between the modules. Obviously, the differences identified in these cases, i.e. 4.6% and 13.0%, are not universal, they can be both smaller and larger depending on the flow conditions and electrical configurations. Nevertheless, both cases clearly show the need for taking the electrical configuration into account when designing systems in which a limited heat source causes temperature distribution among the modules. The multi-scale model presented here allows these effects to be accounted for with a minimum increase in computational demand.

6 CONCLUSIONS

This research contributes with novel modelling and simulation strategies for thermoelectric generators. The work relies to a large extent on simulations that are supported with high quality measurements.

In Paper I, a first principle model was developed and transient simulations were conducted on a TE pair in contact with a small gas channel. The main conclusion from this study was the importance of having good heat transfer on the gas side while maintaining a low pressure drop in order to achieve an overall high power conversion.

Also in Paper II, a first principle model was used. The aim was to develop a method to determine the thermal and electrical contact resistances inside TE modules based on simulations and measurements of module performance. This was shown to be successful, and allowed for high accuracy in predicting module performance over a large range of operating conditions. The contact resistances determined in the analysis were further validated by implementing them in simulations of similar modules but with completely different geometrical dimensions, and also these simulations showed excellent agreement with measurements. It was concluded that the methodology presented in Paper II allows for contact resistances in thermoelectric generators to be determined accurately, and that the effect of contact resistances should always be accounted for in module simulations.

In Paper III, the goal was to develop reduced TE models that can be used to efficiently simulate large system of modules in a CFD analysis. This was achieved by the use of subgrid models that describe the electrical and thermal characteristics of individual modules and an electrical model of the connected system. These models were coupled to a CFD solver which allowed a two-way coupling to be used in the energy equation, i.e. a

simultaneous solution of fluid dynamic and thermoelectric generation allowing Peltier, Thomson, and Joule effects to be accounted for correctly. The models allows for heat flow and electrical power output to be predicted with just a minor increase in computational demand compared to standard CFD models. High quality measurements of module performance were used for developing the simulation models, and the models were validated on a system of modules connected together. Subsequently, validations were done under severe conditions in which the model was extrapolated far outside the measured operating range used for model development, i.e. to conditions with reversed current in which some modules operate as Peltier coolers rather than generators. Consequently, the simulation framework was able to bridge the scale separation problem and allowed for heat flow and electric power generation to be determined accurately.

In Paper IV, the subgrid models developed in this research were used together with CFD to simulate a full-scale prototype of a TEG heat exchanger based on heat pipe technology. In this study, measurements in an engine bench laboratory were used to validate the multiphysics model. Pressure drop, temperature distribution, and electrical power generation were validated, and the agreement between simulations and measurements was excellent. The non-ideal effect that occurs when connected modules operate with different temperature gradients were investigated, and, a potential power loss of up to 13% was found. This is, however, no universal value; other cases could result in even larger deviations between optimal and real power output. By implementing the modelling strategy presented here, these deviations can be fully accounted for and the models can also be used to design heat exchangers with the goal of minimizing these non-ideal effects. It was found that this modelling approach gives very good insight into how heat transfer occurs and how thermoelectric modules should be integrated into heat exchangers for heat recovery in exhaust gas systems. More importantly, the model also allowed for fast and inexpensive concept evaluations by virtual prototyping.

7 FUTURE WORK

Because of the low efficiency of thermoelectric generators, future studies should continue to focus on development of new, and improving existing thermoelectric materials in order to make thermoelectric heat recovery in automotive applications profitable on a large scale. As shown in this thesis, contact resistances have a major negative impact on module performance, and future studies should therefore focus on lowering these resistances to increase module efficiency.

First principle simulations are highly valuable for conceptual studies and for the design of new TE modules, and it is advisable that researchers continue to use first principle models for these purposes. Due to the high computational demand these models require, they should, however, be avoided for the design of large systems of modules incorporated in heat exchangers. For this purpose, it is recommended that the models developed in this work be used instead. The generic formulation of the model allows for different heat exchanger concepts and designs to be evaluated efficiently and with high accuracy. The models presented here can also be used to optimize electrical connections in order to achieve maximum power output and at the same time keep the voltage is at a suitable level. Because of the efficiency of the models, this could possibly be done in line in a control algorithm if the modules are connected in a flexible, transistor-based switching network.

In order to perform transient analysis of large systems of modules, the equations that describe the heat flow in the subgrid model could be expanded to also include an accumulation term. This would be valuable for automotive applications, among others, in which there are a lot of transients in the available thermal energy.

BIBLIOGRAPHY

1. Eurostat, E.C., *Energy, transport and environment indicators*. 2013, European Union: Luxemburg.
2. *REGULATION (EC) No 595/2009 OF THE EUROPEAN PARLIAMENT AND OF THE COUNCIL of 18 June 2009 on type-approval of motor vehicles and engines with respect to emissions from heavy duty vehicles (Euro VI) and on access to vehicle repair and maintenance information and amending Regulation (EC) No 715/2007 and Directive 2007/46/EC and repealing Directives 80/1269/EEC, 2005/55/EC and 2005/78/EC*, T.E.P.A.T.C.O.T.E. UNION, 2009.
3. Nuwayhid, R.Y., A. Shihadeh, and N. Ghaddar, *Development and testing of a domestic woodstove thermoelectric generator with natural convection cooling.* Energy Conversion and Management, 2005. 46(9–10): p. 1631-1643.
4. O'Shaughnessy, S.M., M.J. Deasy, J.V. Doyle, and A.J. Robinson, *Field trial testing of an electricity-producing portable biomass cooking stove in rural Malawi.* Energy for Sustainable Development, 2014. 20: p. 1-10.
5. Champier, D., J.P. Bédécarrats, T. Kousksou, M. Rivaletto, F. Strub, and P. Pignolet, *Study of a TE (thermoelectric) generator incorporated in a multifunction wood stove.* Energy, 2011. 36(3): p. 1518-1526.
6. Py, X., Y. Azoumah, and R. Olives, *Concentrated solar power: Current technologies, major innovative issues and applicability to West African countries.* Renewable & Sustainable Energy Reviews, 2013. 18: p. 306-315.
7. Liao, T.J., B.H. Lin, and Z.M. Yang, *Performance characteristics of a low concentrated photovoltaic-thermoelectric hybrid power generation device.* International Journal of Thermal Sciences, 2014. 77: p. 158-164.
8. Ji, J., J.P. Lu, T.T. Chow, W. He, and G. Pei, *A sensitivity study of a hybrid photovoltaic/thermal water-heating system with natural circulation.* Applied Energy, 2007. 84(2): p. 222-237.
9. Zhang, M., L. Miao, Y.P. Kang, S. Tanemura, C.A.J. Fisher, G. Xu, C.X. Li, and G.Z. Fan, *Efficient, low-cost solar thermoelectric cogenerators comprising evacuated tubular solar collectors and thermoelectric modules.* Applied Energy, 2013. 109: p. 51-59.

10. He, W., Y. Su, S.B. Riffat, J. Hou, and J. Ji, *Parametrical analysis of the design and performance of a solar heat pipe thermoelectric generator unit.* Applied Energy, 2011. 88(12): p. 5083-5089.

11. Suter, C., Z.R. Jovanovic, and A. Steinfeld, *A 1 kWe thermoelectric stack for geothermal power generation – Modeling and geometrical optimization.* Applied Energy, 2012. 99: p. 379-385.

12. Whalen, S.A. and R.C. Dykhuizen, *Thermoelectric energy harvesting from diurnal heat flow in the upper soil layer.* Energy Conversion and Management, 2012. 64: p. 397-402.

13. El-Genk, M.S. and H.H. Saber, *Performance analysis of cascaded thermoelectric converters for advanced radioisotope power systems.* Energy Conversion and Management, 2005. 46(7–8): p. 1083-1105.

14. Kaibe, H., K. Makino, T. Kajihara, S. Fujimoto, and H. Hachiuma, *Thermoelectric Generating System attached to a Carburizing Furnace at Komatsu Ltd., Awazu Plant*, in *9th European Conference on Thermoelectrics*, K.M. Paraskevopoulos and E. Hatzikraniotis, Editors. 2012, Amer Inst Physics: Melville. p. 524-527.

15. Siviter, J., A. Knox, J. Buckle, A. Montecucco, E. McCulloch, and Ieee, *Megawatt scale energy recovery in the Rankine cycle.* 2012 Ieee Energy Conversion Congress and Exposition (Ecce), 2012: p. 1374-1379.

16. Wang, Y., C. Dai, and S. Wang, *Theoretical analysis of a thermoelectric generator using exhaust gas of vehicles as heat source.* Applied Energy, 2013. 112: p. 1171-1180.

17. Högblom, O. and R. Andersson, *CFD Modeling of Thermoelectric Generators in Automotive EGR-coolers* American Institute of Physics Conference Series 2011. 1449: p. 497-500.

18. Espinosa, N., M. Lazard, L. Aixala, and H. Scherrer, *Modeling a Thermoelectric Generator Applied to Diesel Automotive Heat Recovery.* Journal of Electronic Materials, 2010. 39(9): p. 1446-1455.

19. Deng, Y.D., Y. Zhang, and C.Q. Su, *Modular Analysis of Automobile Exhaust Thermoelectric Power Generation System.* Journal of Electronic Materials, 2015. 44(6): p. 1491-1497.

20. Yu, S.H., Q. Du, H. Diao, G.Q. Shu, and K. Jiao, *Start-up modes of thermoelectric generator based on vehicle exhaust waste heat recovery.* Applied Energy, 2015. 138: p. 276-290.

21. Hsu, C.T., G.Y. Huang, H.S. Chu, B. Yu, and D.J. Yao, *Experiments and simulations on low-temperature waste heat harvesting system by thermoelectric power generators.* Applied Energy, 2011. 88(4): p. 1291-1297.

22. Hsu, C.T., D.J. Yao, K.J. Ye, and B. Yu, *Renewable energy of waste heat recovery system for automobiles.* Journal of Renewable and Sustainable Energy, 2010. 2(1): p. 12.

23. Hsiao, Y.Y., W.C. Chang, and S.L. Chen, *A mathematic model of thermoelectric module with applications on waste heat recovery from automobile engine.* Energy, 2010. 35(3): p. 1447-1454.

24. Karri, M.A., E.F. Thacher, and B.T. Helenbrook, *Exhaust energy conversion by thermoelectric generator: Two case studies.* Energy Conversion and Management, 2011. 52(3): p. 1596-1611.

25. Thacher, E.F., B.T. Helenbrook, M.A. Karri, and C.J. Richter, *Testing of an automobile exhaust thermoelectric generator in a light truck.* Proceedings of the Institution of Mechanical Engineers Part D-Journal of Automobile Engineering, 2007. 221(D1): p. 95-107.

26. Chen, M., L.A. Rosendahl, and T. Condra, *A three-dimensional numerical model of thermoelectric generators in fluid power systems.* International Journal of Heat and Mass Transfer, 2011. 54(1–3): p. 345-355.

27. Chen, W.H., C.Y. Liao, and C.I. Hung, *A numerical study on the performance of miniature thermoelectric cooler affected by Thomson effect.* Applied Energy, 2012. 89(1): p. 464-473.

28. Cheng, C.H. and S.Y. Huang, *Development of a non-uniform-current model for predicting transient thermal behavior of thermoelectric coolers.* Applied Energy, 2012. 100: p. 326-335.

29. Ziolkowski, P., P. Poinas, J. Leszczynski, G. Karpinski, and E. Müller, *Estimation of Thermoelectric Generator Performance by Finite Element Modeling.* Journal of Electronic Materials, 2010. 39(9): p. 1934-1943.

30. Hu, X.K., H. Takazawa, K. Nagase, M. Ohta, and A. Yamamoto, *Three-Dimensional Finite-Element Simulation for a Thermoelectric Generator Module.* Journal of Electronic Materials, 2015. 44(10): p. 3637-3645.

31. Rezania, A. and L.A. Rosendahl, *A comparison of micro-structured flat-plate and cross-cut heat sinks for thermoelectric generation application.* Energy Conversion and Management, 2015. 101: p. 730-737.

32. Bjork, R., *The Universal Influence of Contact Resistance on the Efficiency of a Thermoelectric Generator.* Journal of Electronic Materials, 2015. 44(8): p. 2869-2876.

33. Ebling, D., K. Bartholome, M. Bartel, and M. Jagle, *Module Geometry and Contact Resistance of Thermoelectric Generators Analyzed by Multiphysics Simulation.* Journal of Electronic Materials, 2010. 39(9): p. 1376-1380.

34. Sakamoto, T., T. Iida, T. Sekiguchi, Y. Taguchi, N. Hirayama, K. Nishio, and Y. Takanashi, *Selection and Evaluation of Thermal Interface Materials for Reduction of the Thermal Contact Resistance of Thermoelectric Generators.* Journal of Electronic Materials, 2014. 43(10): p. 3792-3800.

35. Martínez, A., J.G. Vián, D. Astrain, A. Rodríguez, and I. Berrio, *Optimization of the Heat Exchangers of a Thermoelectric Generation System.* Journal of Electronic Materials, 2010. 39(9): p. 1463-1468.

36. Edvardsson, J., H. Westberg, J. Dawody, L. Andersson, H. Härelind Ingelsten, H. Kannisto, F. Gunnarsson, A. Palmqvist, R. Heijl, Y. Ma, D. Cederkrantz, R. Andersson, O. Högblom, L.J. Pettersson, X. Karatzas, M.Z. Granlund, P.O. Larsson, L. Holmgren, and F. Andreasson, *E4-Mistra, a research program for the development of an energy efficient low emission exhaust aftertreatment system for heavy duty vehicles*, in *World Renewable Energy Forum, WREF 2012*. 2012: Denver. p. 4530-4536.

37. Rowe, D.M., ed. *CRC Handbook of Thermoelectrics*. 1995, CRC Press LLC: Boca Raton, Florida.

38. Riffat, S.B. and X.L. Ma, *Thermoelectrics: a review of present and potential applications.* Applied Thermal Engineering, 2003. 23(8): p. 913-935.

39. Snyder, G.J. and E.S. Toberer, *Complex thermoelectric materials.* Nat Mater, 2008. 7(2): p. 105-114.

40. G. S. Nolas, J.S., H. J. Goldsmid, *Thermoelectrics: Basic Principles and New Materials Developments*. 2001, Springer: New York.

41. Faleev, S.V. and F. Léonard, *Theory of enhancement of thermoelectric properties of materials with nanoinclusions.* Physical Review B, 2008. 77(21): p. 214304.

42. Ma, Y., R. Heijl, and A.C. Palmqvist, *Composite thermoelectric materials with embedded nanoparticles.* Journal of Materials Science, 2013. 48(7): p. 2767-2778.

43. Fergus, J.W., *Oxide materials for high temperature thermoelectric energy conversion.* Journal of the European Ceramic Society, 2012. 32(3): p. 525-540.

44. Masaki Kazeoka, H.H., *Improvement in Thermoelectric Properties of (ZnO)(5)In2O3 through Partial Substitution of Yttrium for Indium.* Materials Research Society, 1998. 3(3): p. 523-526.

45. Goldsmid, H.J. and R.W. Douglas, *The use of semiconductors in thermoelectric refrigeration.* British Journal of Applied Physics, 1954. 5(11): p. 386.

46. Biswas, K., J. He, I.D. Blum, C.-I. Wu, T.P. Hogan, D.N. Seidman, V.P. Dravid, and M.G. Kanatzidis, *High-performance bulk thermoelectrics with all-scale hierarchical architectures.* Nature, 2012. 489(7416): p. 414-418.

47. DiSalvo, F.J., *Thermoelectric Cooling and Power Generation.* Science, 1999. 285(5428): p. 703-706.

48. Cengel, Y.A., *Heat and Mass Transfer*. 4 ed, ed. A.J. Ghajar. 2011: McGraw-Hill Higher Education.

49. Nagaraju, P.M.a.J., *Electrical Contact Resistance in Thin (≤0.5μm) Gold Plated Contacts: Effect of Gold Plating Thickness.* IEEE TRANSACTIONS ON COMPONENTS AND PACKAGING TECHNOLOGIES, 2010. 33(4): p. 830-835.

50. Chung, D.D.L., *Materials for thermal conduction.* Applied Thermal Engineering, 2001. 21(16): p. 1593-1605.

51. Loulou, T., E.A. Artyukhin, and J.P. Bardon, *Estimation of thermal contract resistance during the first stages of metal solidification process: II—experimental setup and results.* International Journal of Heat and Mass Transfer, 1999. 42(12): p. 2129-2142.

52. Faghri, A., *Heat Pipe Science and Technology*. Mechanical Engineering. 1995, London: Taylor & Francis Group.

53. Wilcox, D.C., *Turbulence Modeling for CFD*. 2006: DCW Industries.

54. Bengt Andersson, R.A., L. Håkansson, M.Mortensen, R.Sudiyo, B.G.M.van Wachem, *Computational Fluid Dynamics for Chemical Engineers*. 2011, Cambridge University Press.

55. Launder, B.E. and B.I. Sharma, *Application of the energy-dissipation model of turbulence to the calculation of flow near a spinning disc.* Letters in Heat and Mass Transfer, 1974. 1(2): p. 131-137.

56. Menter, F.R., *Zonal Two Equation Kappa-Omega Turbulence Models for Aerodynamic Flows*, in *AIAA Fluid Dynamics Conference*. 1993: Orlando, FL; United States.

57. Thayer, J. *Analysis of a heat pipe assisted heat sink*. in *9th International FLOTHERM Users Conference*. 2000. Orlando, Fla, USA.

58. McCarty, R., *A Comparison Between Numerical and Simplified Thermoelectric Cooler Models.* Journal of Electronic Materials, 2010. 39(9): p. 1842-1847.

59. Fraisse, G., J. Ramousse, D. Sgorlon, and C. Goupil, *Comparison of different modeling approaches for thermoelectric elements.* Energy Conversion and Management, 2013. 65(0): p. 351-356.

60. Antonova, E.E. and D.C. Looman. *Finite elements for thermoelectric device analysis in ANSYS*. in *Thermoelectrics, 2005. ICT 2005. 24th International Conference on*. 2005.

61. Gao, X., M. Chen, G.J. Snyder, S. Andreasen, and S. Kær, *Thermal Management Optimization of a Thermoelectric-Integrated Methanol Evaporator Using a Compact CFD Modeling Approach.* Journal of Electronic Materials, 2013. 42(7): p. 2035-2042.

62. Montecucco, A., J. Siviter, and A.R. Knox, *The effect of temperature mismatch on thermoelectric generators electrically connected in series and parallel.* Applied Energy, 2014. 123: p. 47-54.

63. ANSYS, I., *Ansys Fluent User's Guide*. 2013: Canonsburg, USA.

64. Thermonamic. *Ingot specification sheet*. [cited 2013 18 june]; Available from: www.thermonamic.com.

65. Woo, B.C., D.Y. Lee, H.W. Lee, I.J. Kim, S. China Industrial Association Of Power, and S. China Industrial Association Of Power, *Characteristic of maximum power with temperature difference for thermoelectric generator*. Twentieth International Conference on Thermoelectrics, Proceedings. 2001, New York: Ieee. 431-434.

66. Ashari, M.A., A.A.A. Rahman, and S. Sulaiman. *Electrical and Configuration Characterization of Thermoelectric Generator Modules* in *11th European Conference on Thermoelectrics*. 2013. Noordwijk, The Netherlands.

67. Hu, X.K., P. Jood, M. Ohta, M. Kunii, K. Nagase, H. Nishiate, M.G. Kanatzidis, and A. Yamamoto, *Power generation from nanostructured PbTe-based thermoelectrics: comprehensive development from materials to modules.* Energy & Environmental Science, 2016. 9(2): p. 517-529.

68. Rasmuson, A., B. Andersson, L. Olsson, and R. Andersson, *Mathematical Modeling in Chemical Engineering*. 2014, Cambridge: Cambridge University Press.

69. Cederkrantz, D., A. Saramat, G.J. Snyder, and A.E.C. Palmqvist, *Thermal stability and thermoelectric properties of p-type Ba(8)Ga(16)Ge(30) clathrates.* Journal of Applied Physics, 2009.

70. Jääskeläinen, H. and M.K. Khair. *EGR Systems & Components*. 2012; Available from: https://www.dieselnet.com/tech/engine_egr_sys.php.